European Journal of Medicinal Chemistry 210 (2021) 113059

Contents lists available at ScienceDirect

European Journal of Medicinal Chemistry

journal homepage: http://www.elsevier.com/locate/ejmech

Research paper

Pleiotropic prodrugs: Design of a dual butyrylcholinesterase inhibitor and 5-HT_6 receptor antagonist with therapeutic interest in Alzheimer's disease

François-Xavier Toublet [a], Julien Lalut [a], Bérénice Hatat [a, b], Cédric Lecoutey [a], Audrey Davis [a], Marc Since [a], Sophie Corvaisier [a], Thomas Freret [c], Jana Sopková-de Oliveira Santos [a], Sylvie Claeysen [b], Michel Boulouard [c], Patrick Dallemagne [a], Christophe Rochais [a, *]

[a] Normandie Univ, Unicaen, CERMN, 14000 Caen, France
[b] IGF, Univ. Montpellier, CNRS, INSERM Montpellier, France
[c] Normandie Univ, Unicaen, INSERM, Comete, GIP CYCERON, 14000 Caen, France

ARTICLE INFO

Article history:
Received 24 August 2020
Received in revised form
23 October 2020
Accepted 24 November 2020
Available online 3 December 2020

Keywords:
Alzheimer's disease
Prodrugs
Butyrylcholinesterase
5-HT_6 receptors
MTDL

ABSTRACT

Beside acetylcholinesterase, butyrylcholinesterase could be considered as a putative target of interest for the symptomatic treatment of Alzheimer's disease (AD). As a result of complexity of AD, no molecule has been approved since 2002. Idalopirdine, a 5-HT_6 receptors antagonist, did not show its effectiveness in clinical trial despite its evaluation as adjunct to cholinesterase inhibitors. Pleiotropic molecules, known as multitarget directed ligands (MTDLs) are currently developed to tackle the multifactorial origin of AD. In this context, we have developed a pleiotropic carbamate **7**, that behaves as a covalent inhibitor of BuChE (IC_{50} = 0.97 μM). The latter will deliver after hydrolysis, compound **6**, a potent 5-HT_6 receptors antagonist (K_i = 11.4 nM) related to idalopirdine. In silico and in vitro evaluation proving our concept were performed completed with first in vivo results that demonstrate great promise in restoring working memory.

1. Introduction

Alzheimer's disease (AD) is a complex neurodegenerative dementia. During the last years several hypotheses have linked its origin and development to β-amyloid plaque formation, hyperphosphorylation of Tau proteins, metal ions, oxidative stress, neuro-inflammation or cholinergic deficit [1].

Despite all these efforts, drugs on the market only exert symptomatic effect, as it is the case with rivastigmine (**1**) (Fig. 1). This molecule is a pseudo-irreversible dual inhibitor of two cholinergic enzymes: acetylcholinesterase (AChE) and butyrylcholinesterase (BuChE) [2]. These enzymes physiologically regulate acetylcholine (ACh), a neurotransmitter whose concentration decreases during the course of AD and neurodegeneration. These enzymes happen to be a prime target in treatment for the development of AD drugs according to the cholinergic hypothesis [3]. BuChE is an esterase present in the peripheral and central nervous system and its roles in AD are increasingly documented. Indeed, during the evolution of the disease, it has been shown that the level of BuChE increases, thus compensating for the AChE which decreases [4,5]. BuChE hydrolyzes ACh at its catalytic anionic site [6] and several selective inhibitors have been developed in the recent years [7,8].

Abbreviations: AD, Alzheimer's disease; 5-HT, serotonin; 5-HT_xR, 5-hydroxytryptamine X receptors; ACh, acetylcholine; AChE, acetylcholinesterase; ACN, acetonitrile; BBB, blood brain barrier; BuChE, butyrylcholinesterase; BuChEI, butyrylcholinesterase inhibitor; cAMP, cyclic adenosine monophosphate; CCDC, Cambridge crystallographic data center; ChE, cholinesterase; CHX, cyclohexane; CPZ, chlorpromazine; DCM, dichloromethane; DMF, dimethylformamide; DMSO, dimethyl sulfoxide; DTNB, 5,5-dithiobis-(2-nitrobenzoic) acid; EDTA, ethylenediaminetetraacetic acid; HPLC, high-performance liquid chromatography; HRMS, high resolution mass spectra; IC_{50}, half-maximal inhibitory concentration; IP, intraperitoneal; K_i, inhibitor constant; LC-MS, liquid chromatography-mass spectrometry; LD_{50}, median lethal dose; LSD, lysergic acid diethylamide; MAO, monoamine oxidase; MK801, dizocilpine; MTDL, multi-target-directed ligands; PAMPA, parallel artificial membrane permeability assay; PBS, phosphate-buffered saline; Pe, PAMPA effective permeability coefficient; rt, room temperature; SC, subcutaneous; SCOP, scopolamine; THF, tetrahydrofuran.

* Corresponding author. Normandie Univ, Unicaen, CERMN, 14000 Caen, France.
E-mail address: christophe.rochais@unicaen.fr (C. Rochais).

https://doi.org/10.1016/j.ejmech.2020.113059
0223-5234/

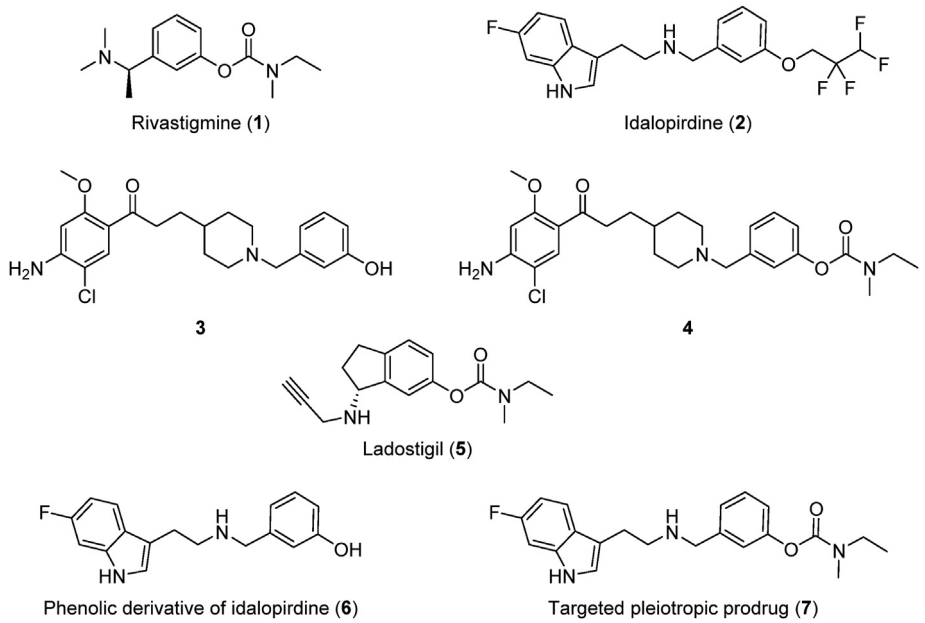

Fig. 1. Structure of rivastigmine (**1**), idalopirdine (**2**), **3**, **4**, ladostigil (**5**), phenolic derivative of idalopirdine (**6**) and targeted pleiotropic prodrug (**7**).

At the same time, new AD targets have been described such as monoamine oxidase [9] and serotonin receptors (G-protein-coupled receptors) 5-HT_4 and 5-HT_6 [10,11]. The 5-hydroxytryptamine 6 (5-HT_6) receptors are involved in several physiological or pathological processes including learning, memory, affective disorders, anxiety, depression, epilepsy and obesity. They are located almost exclusively at the cerebral level: entorhinal and frontal cortex, *hippocampus*, *striatum, amygdala* and *nucleus accumbens* [12]. These receptors induce cAMP production by stimulating the activity of adenylate cyclase. One of the main effects of 5-HT_6R activation is the decrease in cholinergic transmission. Conversely, receptor blockade induces an increase in ACh production, thereby stimulating cholinergic transmission. In AD, it has been shown that patients experience a decrease in the density of these receptors in the cortex. This would be an adaptation mechanism that would prevent a significant fall in ACh [13]. Many 5-HT_6R agonists [14] or antagonists [15] have been developed including idalopirdine (**2**) [16]. This molecule has particular characteristics such as the absence of sulfone, characteristic of the pharmacophore of this receptor. Unfortunately, this promising molecule failed in phase 3 clinical studies and did not shown any real efficacy despite good tolerability [17,18]. Interestingly, an extension study has been conducted in order to evaluate idalopirdine along with donepezil to treat mild and moderate form of AD [19], demonstrating the potential synergistic effect to act simultaneously on 5-HT_6R and ChE [20].

Faced with these failures, a new concept has been developed, the MTDLs, thus allowing a molecule to interact with several therapeutic targets [21] in order to tackle the multifactorial origin of AD [22]. Many molecules have been developed in recent years acting on several targets of interest in the context of AD [23] such as donecopride [24–26], but limited examples have been developed targeting ChE as well as GPCR such as serotonin receptors [27–30].

In order to complement the traditional possibility to conceive MTDL by linking [22], fusing or merging structure, we have recently prepared pleiotropic prodrug [31]. A new molecule has been described that allows the release of a 5-HT_4R agonist (**3**) at the cerebral level after activation by AChE [31]. This molecule **4** can inhibit AChE and release an active compound on a second therapeutic target (Fig. 2). AChE, being inhibited during this hydrolysis, can be considered in this case both as a therapeutic target and as an activating enzyme. This molecule was inspired by ladostigil (**5**) (Fig. 1), the first pleiotropic anti-AD prodrug molecule reported in the literature. It possesses a carbamate moiety which is able to covalently bind to AChE and to liberate a hydroxy derivative of rasagiline, displaying Monoamine Oxidase (MAO)-B inhibitory activity [32–34].

In the present work, we wished to develop a new pleiotropic prodrug able to inhibit cholinesterases (ChE) and then to release active metabolite related to idalopirdine (**2**) while keeping its potent 5-HT_6R activity. This compound will be designed based on the model of structurally related rivastigmine (**1**), which covalently binds and inhibits AChE and BuChE.

In order to reach this goal we proposed to prepare and evaluate a novel carbamate analogue (**7**) of idalopirdine. The capacity of the latter to inhibit ChE in a covalent manner was investigated as well as the ability of the carbamate to release the corresponding phenol. The new phenolic derivative (**6**) will be an analogue of idalopirdine, and therefore its ability to interact with 5-HT_6R and its pharmacological profile will be determined and compared with idalopirdine. Finally, in vivo tests have been performed with both analogues in order to provide, for this pleiotropic prodrug, a pro-cognitive effect.

2. Results and discussion

2.1. Chemistry

The targeted phenolic derivative of idalopirdine (**6**) and his carbamate (**7**) were obtained starting from 6-fluoroindole (**8**). First precursor (**11**) was synthesized in three steps, through the following sequence (Scheme 1), described by Muratore et al. [35]. 6-Fluoroindole (**8**) was submitted to a Vilsmeier-Haack reaction to obtain aldehyde (**9**) in position 3 in 94% yield. Henry reaction was then performed to afford nitrated compound (**10**), which was finally reduced by $LiAlH_4$ to obtain the fluorotryptamine **11** in 40% yield.

In parallel, benzaldehydes **13**–**15** were synthesized (Scheme 2).

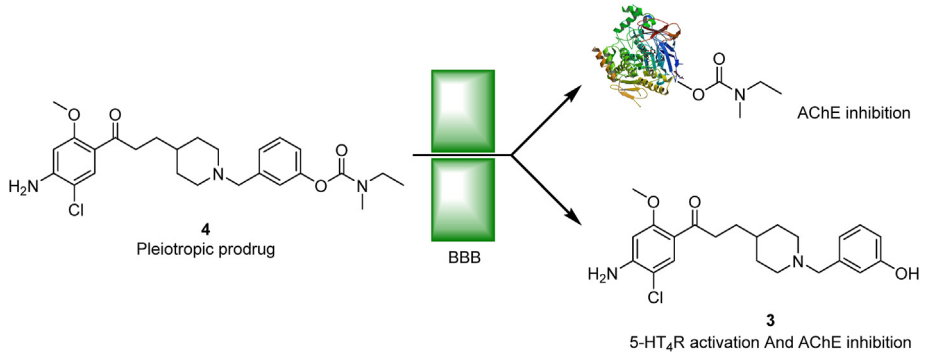

Fig. 2. Illustration of mechanism of action of the pleiotropic prodrug related to donecopride [31].

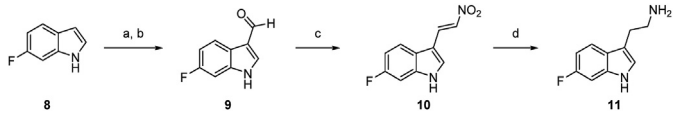

Scheme 1. Synthesis of compound **11**. Reagents and conditions: (a) $POCl_3$, DMF, rt, 3 h; (b) KOH, reflux, 3 h, 94% for to steps; (c) NH_4OAc, $MeNO_2$, reflux, 1 h, 52%; (d) $LiAlH_4$, THF, rt, 3 h, 40%.

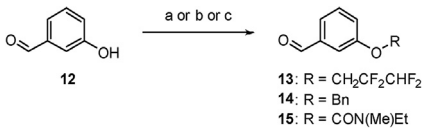

Scheme 2. Synthesis of the compound **13**–**15**. Reagents and conditions: (a) 1,1,2,2-tetrafluoro-3-iodopropane, K_2CO_3, DMF, 80 °C, 1 h: **13**, 53%; (b) Benzyl bromide, K_2CO_3, acetone, rt, 21 h: **14**, 66%; (c) *N*-ethyl-*N*-methylcarbamoyl chloride, K_2CO_3, DMF, 80 °C, 1 h: **15**, 87%.

Compound **13** was synthesized from 3-hydroxybenzaldehyde (**12**) and 1,1,2,2-tetrafluoro-3-iodopropane. **12** was protected with benzyl bromide to yield compound **14**. Finally, **12** was carbamoylated using ethylmethylcarbamic chloride to obtain the carbamate **15** [31].

The targeted compounds **2**, **16** and **7** were finally obtained by reductive amination between **11** and **13**, **14** or **15** (Scheme 3) Compound **16** was deprotected by hydrogenolysis to yield phenol derivative **6**. Finally, the fumaric salts of compounds **6** and **7** were prepared using fumaric acid in *i*PrOH.

2.2. In vitro results

2.2.1. ChE inhibition and 5-HT$_6$R binding

The synthesized phenolic derivative and its carbamate analogue were evaluated as potential inhibitors of human AChE and BuChE, using the Ellman assay [36], as well as potential ligands for human 5-HT$_6$R using a radioligand displacement assay. In these tests, donepezil was used as a reference AChE inhibitor (AChEI), tacrine and rivastigmine (**1**) were used as reference BuChE inhibitor (BuChEI), and SB271046 as a reference 5-HT$_6$R antagonist [16]. The results are depicted in Table 1.

Carbamate **7** appeared able to inhibit BuChE with IC_{50} value in submicromolar on the contrary to the corresponding phenolic derivative **6**, which has limited activity toward this enzyme. In the same assay carbamate **7** and phenol **6** demonstrated limited inhibition properties toward AChE with a selectivity index of 18 in favor of BuChE. Concerning 5-HT$_6$R affinity, carbamate **7** appeared to be devoid of such activity, while its phenolic analogue **6** appeared to be a potent ligand with a K*i* value in the same range as SB271046 and idalopirdine (**2**). Moreover, the activity of the fumarate salts **17** and **18** were similar to their corresponding bases.

2.2.2. Pharmacological profile results

The pharmacological profile of the selected phenolic derivative **17** and **18** were first established towards *h*5-HT$_6$R. As expected, due to its low affinity compound **18** demonstrated no activity (see Supporting Information). Compound **17** acts as an antagonist in a similar manner as idalopirdine (**2**) (Fig. 3 and Table 2).

On the other hand, the mechanism of equine BuChE (*eq*BuChE) inhibition for compound **18** was evaluated by means of a kinetic study, the results of which are reported in typical Lineweaver-Burk plots. Carbamate **18** showed a mixed-type inhibition (Fig. 4),

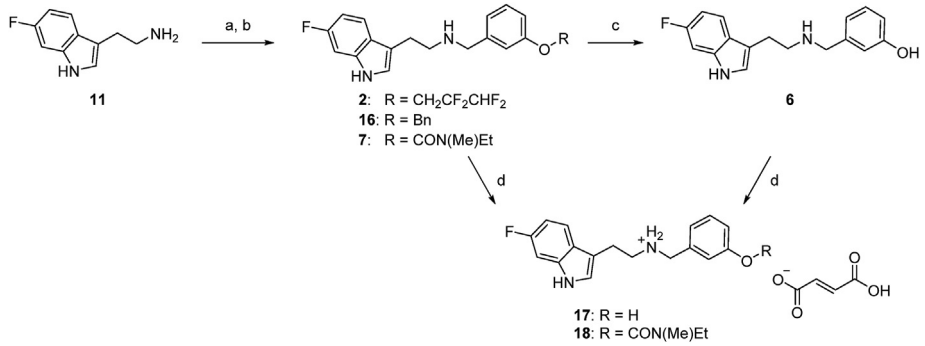

Scheme 3. Synthesis of compounds **2, 6** and **7**. Reagents and conditions: (a) **11**, **12** or **13**, AcOH, MeOH, rt, 18 h, 5–54%; (b) $NaBH_4$, rt, 1 h; (c) Start to **16**, H_2, Pd/C, rt, 72 h, 37%; (d) **6** or **7**, fumaric acid, iPrOH, reflux, 1 h, 63–73%.

Table 1
*h*AChE and *h*BuChE inhibitory Activity (% inhibition or IC_{50}) and *h*5-HT_6R affinity (% inhibition or K_i).

Compound	R	*h*AChE		*h*BuChE		Selectivity index[b]	*h*5-HT_6R	
		% Inhibition at 10^{-6} M	IC_{50} (nM)[a]	% Inhibition at 10^{-5} M	IC_{50} (nM)[a]		% Inhibition at 10^{-6} M/10^{-8} M	K_i (nM)[c]
Donepezil	–	–	7.0 ± 1.5	–	–	–	–	–
Tacrine	–	–	–	–	85 ± 6		–	–
Rivastigmine (**1**)[d]	–	–	4150 ± 160	–	37 ± 5	0.01	–	–
SB271046[e]	–	–	–	–	–	–	–	3.0 ± 0.7
2	$CH_2CF_2CHF_2$	6	ND[f]	–	ND	–	106/88	6.9 ± 1.2
16	Bn	4	ND	2	ND		103/14	ND
6	H	8	ND	11	ND	–	104/33	11.4 ± 4.4
7	CON(Me)Et	9	16,500 ± 3900	93	927 ± 81	0.06	37/24	ND
17	H, fumaric salt	2	ND	8	ND	–	85/48	4.3 ± 0.8
18	CON(Me)Et, fumaric salt	5	17,555 ± 1916	97	835 ± 44	0.05	53/32	ND

[a] IC_{50} and values are expressed as mean ± standard error of the mean (SEM) of at least two experiments.
[b] Selectivity index = IC_{50}(*h*BuChE)/IC_{50}(*h*AChE).
[c] K_i and values are expressed as mean ± standard error of the mean (SEM) of at least three experiments.
[d] Data from Ref. [37].
[e] Data from Ref. [16].
[f] ND: not determined.

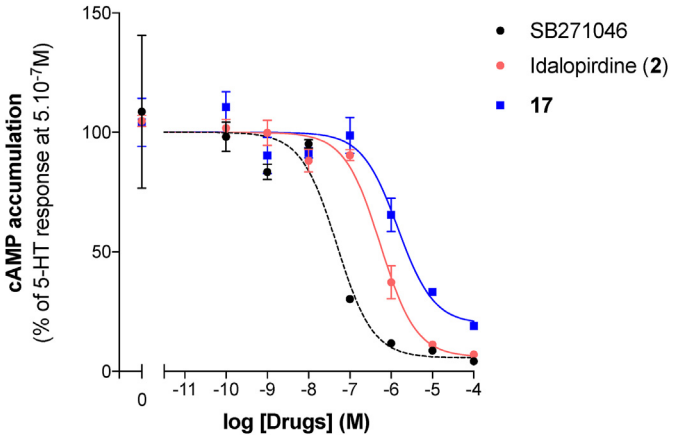

Fig. 3. Pharmacological profiles of idalopirdine (**2**) and compound **17**. Representative experiment illustrating antagonist activities towards *h*5-HT_6 receptors.

Table 2
*h*5-HT_6 pharmacological profiles of idalopirdine (**2**) and compound **17**. SB271046 was used as a control 5-HT_6R antagonist.

Compound	log (IC_{50})[a]	% control antagonist response	Profile
2	−6.0 ± 0.9	100.7 ± 1.29	antagonist
17	−5.7 ± 0.2	87.2 ± 4.45	antagonist

[a] Log (IC_{50}) and % control antagonist response values are expressed as mean ± standard error of the mean (SEM) of three experiments.

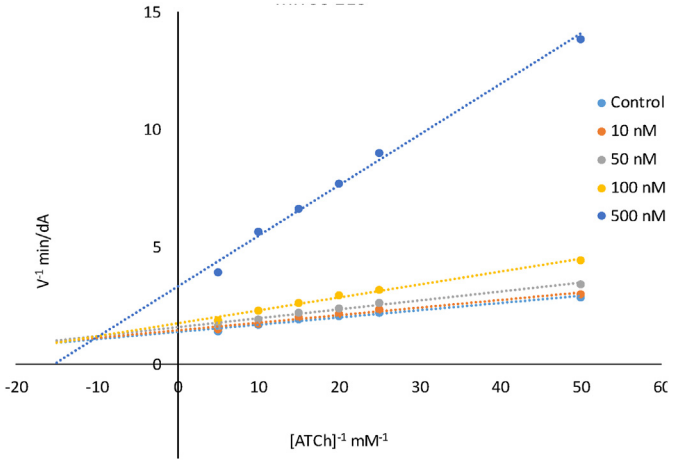

Fig. 4. Lineweaver-Burk plots of inhibition kinetics show that carbamate **18** acts as a mixed-type *eq*BuChE inhibitor.

illustrated by a typical Lineweaver-Burk plot similar to those obtained with the covalent BuChEI, rivastigmine [38].

2.2.3. Brain penetration

The ability of carbamate **18** to cross the blood brain barrier (BBB) was assessed using a parallel artificial membrane permeability assay experiment (PAMPA). The compound was classified among the compounds having good brain penetration with logPe = −4.44 (Pe represents the PAMPA effective permeability coefficient). The test was performed using good (corticosterone) and weak brain-penetrating references (theophylline), respectively (Table 3).

Table 3
LogPe represents the PAMPA effective permeability coefficient results for **18** and reference compounds.

Compound	log (IC_{50})
Corticosterone	−4.80 ± 0.02
Theophylline	−6.35 ± 0.02
18	−4.44 ± 0.07

carbonyl and hydroxy group of Ser198 was applied during the docking procedure and the Ser198 side chain was kept flexible at the same time. In all generated poses the carbamate moiety was located near the catalytic triad as imposed by the constraint and the ligand indole ring was placed close to peripheral anionic site. The ChemPLP score fit values of generated poses of compound **18** varied between 87.65−77.80. These values were comparable to the

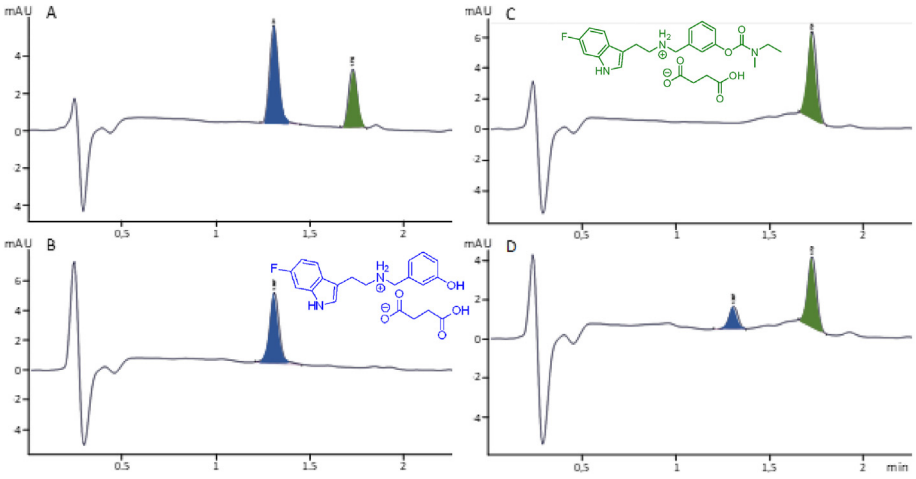

Fig. 5. Decarbamoylation of **18** by *eq*BuChE; (A): **18** (5 μM) and **17** (5 μM) calibration range; (B): **18** (5 μM) without *eq*BuChE (negative control); (C): **17** (5 μM) without *eq*BuChE (negative control); (D): **18** (5 μM) in the presence of 250 U/mL *eq*BuChE; 25 °C, 18 h, λ = 280 nm.

2.2.4. *BuChE-dependent decarbamoylation*

The stability of the carbamate **18** in buffer or in presence of BuChE and its possible in vitro decarbamoylation were tested. We used in this aim a new analytical method described by Alix et al. [39] and developed for compound **5** [31]. Owing to its high homology with the active-site sequence of the human BuChE and its commercial availability, butyrylcholinesterase form equine source (*eq*BuChE) is commonly used for in vitro assays and was chosen for this study. A large excess of *eq*BuChE was added to a solution of **18** in a phosphate-buffered saline (PBS) buffer (pH 7.4) at 25 °C. After 24 h of incubation, the solution was extracted by ethyl acetate, evaporated and the residue was solubilized in acetonitrile, and then analyzed by HPLC and LC-MS.

Four analyzes were conducted. A first calibration range was performed in presence of **17** and **18** (Fig. 5A). Then the control experiments in a PBS buffer without *eq*BuChE, under the same reaction conditions, was also performed to ensure the stability of **17** in buffer (Fig. 5B) and **18** which was not chemically converted into **17** (Fig. 5C). On the contrary, when *eq*BuChE was added to the solution, a decarbamoylation of **18** and the release of **17** was observed (Fig. 5D).

2.3. *In silico results*

Docking studies were performed using GOLD v5.7.2 (v5.7.2, Cambridge Crystallographic Data Center, CCDC), in order to predict the ability of **18** to interact with *h*BuChE binding site. We wished to check if the carbamate derivative **18** could access the *h*BuChE catalytic triad, especially the Ser198 residue playing the crucial role during the carbamoylation. According to the proposed carbamoylation mechanism of rivastigmine by Bacalhau et al. [40], the carbamate-to-serine grouping approach starts *via* a hydrogen bond between oxygen atom of carbamate carbonyl and hydroxy group of Ser198. This is why a hydrogen bond constraint between carbamate ChemPLP score fit obtained for the ligand from original crystallographic complex (87.20). The generated poses of **18** could be divided in two clusters (Fig. 6). In the first cluster (Fig. 6A), the ligand adopts a curve conformation and the indole ring created a π-π stacking with Tyr332 residue of the peripheral anionic site. Furthermore, a hydrogen bond is formed between the ligand protonated amine and carbonyl group of Pro285 backbone. In cluster 2, the ligand takes a similar position at the bottom of the binding site. The H bond between the protonated amine and the carbonyl group of Pro285 backbone is also conserved. However, the ligand conformation is elongated in cluster 2 (Fig. 6B) and indole moiety point into the entrance to the binding site cavity without establishing a particular interaction.

To evaluate the relevance of these two poses, dynamics simulations of 50 ns were carried out on each representative docking poses. The representative complex structure selected using κ-clustering from each molecular dynamics trajectory are presented in Fig. 6C and D. We have observed that the docking pose 1 was less stable. The ligand changed its conformation during this dynamic to the elongated one, similar to the second pose observed in docking study, and it lost both hydrogen contacts, with Pro285 as well as with Ser198. The docking pose 2 was more stable along our molecular dynamic simulations. The hydrogen bond with Pro285 was preserved and ligand carbonyl group stayed close enough the Ser198 (4.6 Å). In conclusion, the elongated conformation of the ligand seems be preferential one and the H bond with Pro285 seems be important for the ligand binding in addition to carbamate interaction.

2.4. *In vivo results*

2.4.1. *Pharmacological evaluation*

Some in vivo investigations have been performed on the selected phenol **17** and its precursor carbamate **18**.

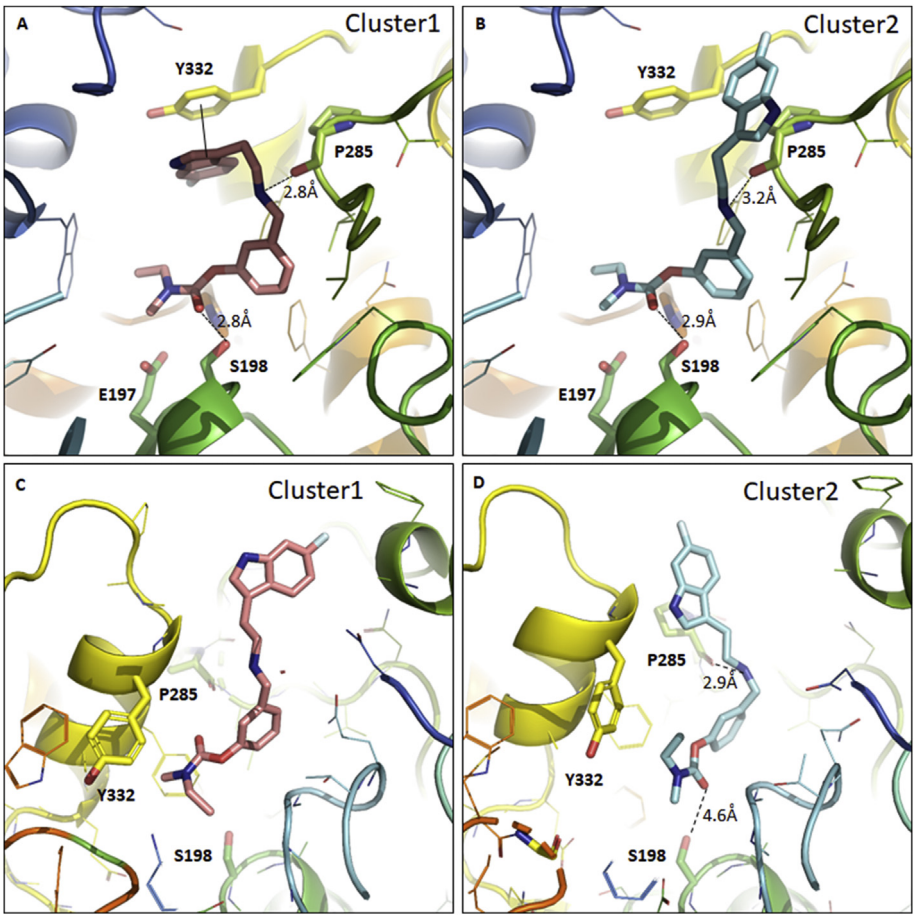

Fig. 6. The two representative positions of compound **18** in *h*BuChE binding sites generated from the docking studies, cluster 1 (**A**) and cluster 2 (**B**) and the representative structure from their molecular dynamics simulations, cluster 1 (**C**) and cluster 2 (**D**). The compound and the selected side chains of the binding site residues are in stick and the protein in ribbon representation. This figure was made with PYMOL (DeLano Scientific, 2002, San Carlo, USA).

Table 4
Pharmacological and toxicological properties of compounds **17** and **18**.

Compound	Dose (mg/kg)	LD_{50} (mg/kg)	Symptoms (Subtoxic doses)
17	1−10 − 100	>100	No symptoms
18	1−10 − 100	>100	No symptoms
Amphetamine[a]	2	–	Hyperactivity, exophtalmy, irritability
Chlorpromazine[a]	10	–	Hypoactivity, ataxia, sleep

[a] Amphetamine (2 mg/kg), chlorpromazine (10 mg/kg) were used as stimulant and depressive references, respectively.

2.4.2. Pharmacological screening

None of the dose tested (1, 10 and 100 mg/kg) for compounds **17** and **18** did show any deleterious signs, suggesting thus a LD_{50} quite higher than 100 mg/kg (Table 4).

2.4.3. Spontaneous locomotor activity

ANOVA revealed a group effect ($F(7,56) = 6.299$, $p < 0.0001$). At the difference of chlorpromazine-treated animals (used as reference drug, $p < 0.0001$), none of the tested doses of compounds **17** and **18** (1, 3 and 10 mg/kg) did statically modify spontaneous locomotor activity in comparison to NaCl-treated control animals (Fig. 7).

2.4.4. Spontaneous alternation deficit

On the basis of the absence of modification of the spontaneous activity performance at the 3 doses tested for compounds **17** and **18**, the latter were studied at the dose of 10 mg/kg in the spontaneous alteration test using Y maze. Whatever the pharmacological agent used to induce a cognitive deficit (scopolamine − SCOP or dizocilpine, MK801), ANOVA of percentage of spontaneous alternation revealed a group effect (respectively, $F(3,32) = 9.2.242$; $p = 0.0002$ and $F(3,32) = 4.631$; $p = 0.0094$) (Fig. 8). In both cases, control group displayed alternation percentage significantly higher than any other animals groups.

In the scopolamine-induced working memory deficit conditions, compound **17** failed to reverse scopolamine-induced deficit. Compound **18** demonstrated a different action profile under this condition. Indeed, if the percentage of alternation of the group (scopolamine-derivative **18**) is significantly different from the control group, univariate *t*-test revealed that only control group and animal having received compound **18** displayed an alternation percentage significantly different from value of the chance level (*i.e.* 50%). Hence, those results point out the ability of the compound **18** to offset − at least partially − scopolamine-induced working

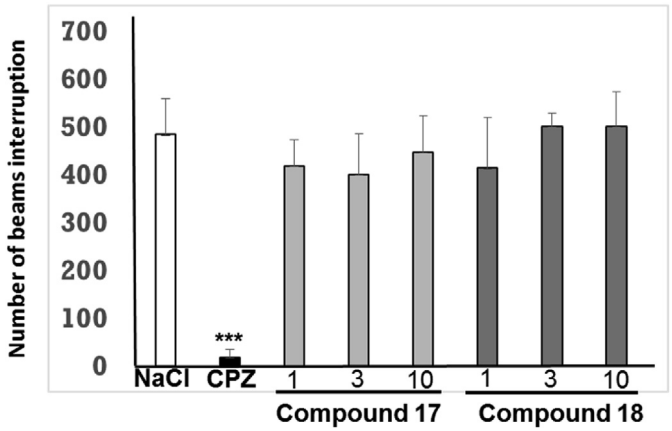

Fig. 7. Effect of compounds **17** and **18** on spontaneous locomotor activity. Data are expressed as the mean ± standard error of mean (SEM, n = 8 per group). Drugs were administered intraperitoneally (IP) 30 min before the behavioral test. Compounds **17** and **18**: 1–3–10 mg/kg; CPZ: chlorpromazine 3 mg/kg (***$p < 0.001$ versus NaCl, SNK test).

memory deficits (Fig. 8A).

The results were found to be different under the conditions of glutamatergic hypofunctioning (MK801-induced deficit) with the absence of effect of compound **18** and demonstration of the ability of compound **17** to partially counterbalance working memory deficit (Fig. 8B). This being attested by univariate *t*-test (alternation percentage significantly different from value of chance).

Overall, beyond the intensity of the effects measured, these data highlight a different in vivo pharmacological profile at the dose tested between phenol **17** and its carbamate analogue **18** in this test.

3. Discussion

The structure of benzylaminephenoxy moiety present in the structure of the 5-HT_6R antagonist idalopirdine **2**, represents an opportunity to apply the ChE prodrug strategy already developed for 5-HT_4R partial agonist in our group [31]. To validate this hypothesis, we would like first to assess the importance of the tetrafluoropropyl chain for 5-HT_6R affinity as well as drugability. In this aim the corresponding phenol **6**, idalopirdine **2** and its ethylmethylcarbamate analogue **7** were prepared using efficient synthesis. Interestingly the in vitro affinity of phenol **6** for 5-HT_6R appears in the nanomolar range, comparable to idalopirdine **2** (Table 1). The removal of the tetrafluoropropyl chain did not affect the profile of the 5-HT_6R ligand **6** (under its fumaric salt form **17**) as this compound demonstrated an antagonist profile in cells overexpressing 5-HT_6R (Fig. 3). However, the introduction of the carbamate group on the phenol **6** appeared particularly detrimental for 5-HT_6R affinity as compound **7** was devoid of affinity for the receptor (Table 1).

In order to be considered as a putative prodrug according to our strategy, we then decided to verify the inhibition properties of the carbamate **7** towards ChE. In vitro assay demonstrated the micromolar inhibition of compound **7** for *h*BuChE with limited activity toward *h*AChE. In the same assay compounds **2** and **6** appeared devoid of activity, suggesting that this property is linked to the presence of the carbamate group on the aromatic region. In order to verify now the possible covalent pseudo-irreversible inhibition of BuChE we first conducted a docking study. Two main clusters were generated but, in both cases, we demonstrated that the carbamate moiety could access the *h*BuChE catalytic triad placing its carbonyl group facing Ser198, the key residue for carbamoylation process (Fig. 6). This position in the active site was also confirmed using a molecular dynamic study. Experimentally, a kinetic study was performed with carbamate **18** which could be described as a mixed-type BuChE inhibitor (Fig. 4) as well as the reference rivastigmine [38]. We then decided to evaluate the stability of the phenol and the carbamate in the presence of the enzyme in buffer. In this experiment, we verified that the carbamate **18** is stable after 18 h in buffer at room temperature and could liberate the corresponding phenol **6** when exposed to the presence of BuChE in the media (Fig. 5). Those experimental data are in favor of the status of the carbamate **18** as a potential pleiotropic prodrug and we then decided to evaluate its activity in in vivo models of AD.

The drugability of **18** was firstly verified and this compound appears as able to cross the BBB in the PAMPA assay. Further, both phenol **17** and carbamate **18** did not statically modify spontaneous locomotor activity in vivo (Fig. 7) and were then selected for in vivo studies to evaluate their antiamnesic effect in two models of induce cognitive impairments. At the dose of 10 mg/kg, carbamate **18** was the only compound able to partially reverse the scopolamine-induced working memory deficits (Fig. 8A), as already demonstrated by rivastigmine in such assay [41]. This result appears as a proof of concept for our study. However, in the MK801 model, the phenol **17** was able to counterbalance the glutamatergic deficit presumably linked to its 5-HT_6R affinity (Fig. 8B). Interestingly, rivastigmine as well as the carbamate **18**, used under similar conditions, proved to be ineffective in improving memory deficits induced by MK801 [42]. The absence of effect of rivastigmine or **18** in this assay could be attributed to a potential effect of MK801 on BuChE. MK801 was evaluated in vitro in the Ellman assay and we

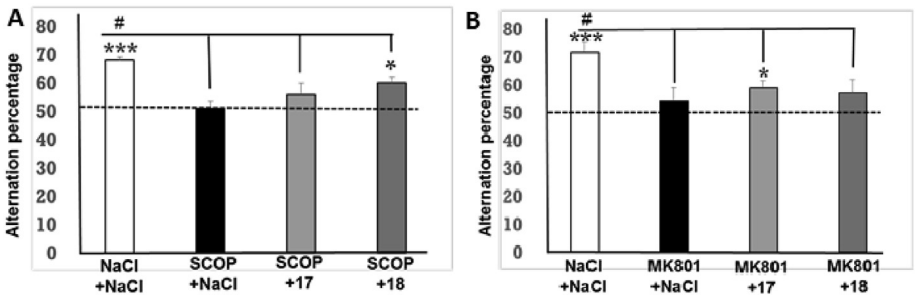

Fig. 8. (**A**) Effect of compounds **17** and **18** on scopolamine impairment during the spontaneous alternation test. Data are expressed as the mean ± standard deviation (SEM, n = 9 per group) NaCl and compounds **17** and **18** (10 mg/kg) were administered IP 30 min before the test, scopolamine (SCOP, 0.5 mg/kg) was administered SC 20 min before the test. (*$p < 0.05$, ***$p < 0.001$ versus 50%; univariate *t*-test). (#p < 0.05 versus other groups, SNK test). (**B**) Effects of compounds **17** and **18** on MK801 induced impairment during the spontaneous alternation test. Data are expressed as the mean ± standard deviation (SEM, n = 9 per group). NaCl and compounds **17** and **18** (10 mg/kg) were administered IP 30 min before the test, MK801 (0.1 mg/kg) was administered SC 20 min before the test. (*$p < 0.05$ versus 50%; univariate *t*-test). (#$p < 0.05$ versus MK801, SNK test).

demonstrated for the first time that MK801 is able to inhibit BuChE with an IC_{50} of 16 μM ± 3, without activity on AChE. Such an effect could potentially affect the activation of the prodrug **18** to explain the difference of activities between the two different models.

4. Conclusion

The recent clinical trials performed with idalopirdine have demonstrated a potential synergy to modulate simultaneously ChE as well as 5-HT_6R in the context of AD. Beside the possible combination of drugs, we decided to investigate the possibility to generate potential MTDLs for those two targets using a prodrug approach. The preparation of a carbamate analogue of idalopirdine, led to a selective in vitro BuChE inhibitor able to release a potent phenolic 5-HT_6R antagonist. The prodrug **18** possesses good drug-ability parameters and appears able in vivo to reverse memory deficit induced by scopolamine. These preliminary studies should be confirmed with further evaluation but confirm the potential to generate a polypharmacology approach using a prodrug strategy.

5. Methods

5.1. Chemistry

5.1.1. General methods

All chemical reagents and solvents were purchased from commercial sources and used without further purification. Melting points were determined on a STUART SMP50 melting point apparatus. ^{1}H, ^{13}C and ^{19}F NMR spectra were recorded on a BRUKER AVANCE III 400 MHz with chemical shifts expressed in parts per million (in chloroform-*d*, methanol-d_4 or DMSO-d_6) downfield from TMS as an internal standard and coupling in Hertz. IR spectra were recorded on a PerkinElmer BX FT-IR apparatus using KBr pellets. High resolution mass spectra (HRMS) were obtained by electrospray on a BrukermaXis. The purities of all tested compounds were analyzed by LC−MS, with the purity all being higher than 95%. Analyses were performed using a Waters Alliance 2695 as separating module (column XBridge C18 2.5 μM/4.6 × 50 mM) using the following gradients: A (95%)/B (5%) to A (5%)/B (95%) in 4.00 min. This ratio was hold during 1.50 min before returning to initial conditions in 0.50 min. Initial conditions were then maintained for 2.00 min (A = H_2O, B = CH_3CN, each containing HCOOH: 0.1%). MS were obtained on a SQ detector by positive ESI. X-ray diffraction experiments: Single crystal X-ray analyses were carried out using graphite-monochromatized Mo Kα radiation on a Bruker-Nonius Kappa II diffractometer equipped with a CCD area detector or on BRUKER D8 Quest diffractometer with a PHOTON2 detector. The crystal structure was solved by direct methods using the SHELX97 package [43] and refined using SHELXL [44]. The refinement was based on F^2 for all reflections, and all non-hydrogen atoms were refined anisotropically. Hydrogen atom positions were determined either *via* difference Fourier maps and refined with isotropic atomic displacement parameters or were calculated and fixed in ideal geometry, depending on data quality.

5.1.2. Synthesis of compounds 9–11 and 13–15

6-fluoro-1H-indole-3-carbaldehyde ***9*** [35]. Phosphorus oxychloride (3.45 mL, 37.0 mmol, 2.5 equiv) was added dropwise to DMF (17 mL) at 0 °C. After 5 min, 6-fluoroindole **8** (2.0 g, 14.8 mmol, 1.0 equiv) in DMF (20 mL) was added. The mixture was stirred for 3 h at room temperature, on a solution of potassium hydroxide 3.8 M (39 mL, 10.0 equiv) was added *via* a dropping funnel at 0 °C. The mixture was stirred at reflux for 3 h. The reaction was cooled down and quenched by saturated aqueous $NaHCO_3$ and EtOAc until the mixture became clear and the organic layer separated. The aqueous layer was extracted with EtOAc and the combined organic layers were dried over $MgSO_4$, filtered and concentrated *in vacuo* to furnish the compound **9** as an orange powder that required no further purification (2.27 g, 94% yield). M. 168 °C; ^{1}H NMR (MeOD, 400 MHz, 295 K): 9.85 (s, 1H), 8.11 (dd, 1H, J = 8.7, 5.6 Hz), 8.06 (s, 1H), 7.17 (dd, 1H, J = 9.4, 2.2 Hz), 7.00 (dd, 1H, J = 9.7, 8.7, 2.2 Hz); ^{13}C NMR (MeOD, 100 MHz, 295 K) δ 187.2, 161.9 (d, J = 238.8 Hz), 140.1 (d, J = 1.5 Hz), 139.0 (d, J = 12.4 Hz), 123.4 (d, J = 9.8 Hz), 122.1, 120.0, 118.8 (d, J = 24.3 Hz), 99.4 (d, J = 26.3 Hz); ^{19}F NMR (MeOD, 374 MHz, 295 K) δ −120.3 (td, J = 9.5, 5.6 Hz).

6-fluoro-3-[(E)-2-nitrovinyl]-1H-indole ***10*** [35]. **9** (2.95 g, 18.1 mmol, 1.0 equiv) and ammonium acetate (4.18 g, 54.26 mmol, 3.0 equiv) were refluxed in nitromethane (59 mL) for 1 h. The solvent was removed *in vacuo* and the crude was dissolved in EtOAc, then the organic layer was washed with brine, dried over $MgSO_4$ and concentrated *in vacuo*. After a purification by flash chromatography on silica gel column (CHX/EtOAc, gradient 100:0 to 70:30), the compound **10** was obtained as a yellow oil (1.95 g, 52% isolated yield). ^{1}H NMR ($CDCl_3$, 400 MHz, 295 K) δ 8.33 (d, 1H, J = 13.4 Hz), 7.91 (s, 1H), 7.87 (d, 1H, J = 13.4 Hz), 7.80 (dd, 1H, J = 8.8, 5.0 Hz), 7.19 (dd, 1H, J = 9.4, 2.3 Hz), 7.04 (dd, 1H, J = 9.6, 8.8, 2.3 Hz); ^{13}C NMR ($CDCl_3$, 100 MHz, 295 K) δ 161.8 (d, J = 239.0 Hz), 139.7 (d, J = 12.3 Hz), 136.4 (d, J = 2.2 Hz), 135.0, 133.0, 122.7, 122.4 (d, J = 10.2 Hz), 111.2 (d, J = 24.5 Hz), 110.1, 99.8 (d, J = 26.2 Hz); ^{19}F NMR ($CDCl_3$, 374 MHz, 295 K) δ −121.1 (td, J = 9.7, 5.0 Hz).

2-(6-fluoro-1H-indol-3-yl*)éthanamine* ***11*** [35]. To a solution of **10** (768 mg, 3.72 mmol, 1.0 equiv) in THF (37 mL) was added to a stirred slurry of $LiAlH_4$ (848 mg, 22.35 mmol, 6.0 equiv) in THF (37 mL) at 0 °C. The mixture was stirred for 3 h at room temperature. The reaction was then slowly quenched at 0 °C with 0.9 mL of water, 0.9 mL of 15% NaOH solution followed by 2.7 mL of water to afford a granular inorganic precipitate. After the night, the solution was filtered over a pad of Celite, the solid was washed with EtOAc, then the filtrate was concentrated *in vacuum*. After a purification by flash chromatography on silica gel column (DCM/MeOH, gradient 100:0 to 90:10), the compound **11** was obtained as a brown oil (264 mg, 40% isolated yield).^{1}H NMR ($CDCl_3$, 400 MHz, 295 K) δ 8.76 (br s, 1H), 7.49 (dd, 1H, J = 8.7, 5.4 Hz), 7.01 (dd, 1H, J = 9.7, 2.2 Hz), 6.97 (s, 1H), 6.88 (dd, 1H, J = 9.6, 8.7, 2.2 Hz), 3.03 (t, 2H, J = 6.6 Hz), 2.88 (t, 2H, J = 6.6 Hz), 1.49 (s, 2H);^{13}C NMR ($CDCl_3$, 100 MHz, 295 K) δ 160.0 (d, J = 237.2 Hz), 136.4 (d, J = 12.4 Hz), 124.2, 122.5 (d, J = 3.5 Hz), 119.6 (d, J = 10.2 Hz), 113.6, 108.0 (d, J = 24.5 Hz), 97.5 (d, J = 25.9 Hz), 42.3, 29.4; ^{19}F NMR ($CDCl_3$, 374 MHz, 295 K) δ −121.5 (td, J = 9.6 Hz, J = 5.4 Hz).

3-(2,2,3,3-tetrafluoropropoxy)benzaldehyde ***13***. K_2CO_3 (6.79 g, 49.13 mmol, 3.0 equiv) was added to a solution of 3-hydroxybenzaldehyde (1.0 g, 8.19 mmol, 1.0 eq) in DMF (70 mL), with an ice bath cooling. After 5 min, the 1,1,2,2-tetrafluoro-3-iodopropane (1.4 mL, 12.28 mmol, 1.5 equiv) was added in the mixture. The solution was then stirred for 2 h at 70 °C. After concentrating the mixture *in vacuo*, the crude was dissolved with EtOAc, then the organic layer was washed with brine, dried over $MgSO_4$ and concentrated *in vacuo*. The crude was purified by chromatography on silica gel column (CHX/EtOAc, gradient 100:0 to 95:5) and concentrated under reduced pressure to afford the compound **13** as a colorless oil (815 mg, 54% isolated yield). ^{1}H NMR ($CDCl_3$, 400 MHz, 295 K) δ 9.98 (s, 1H), 7.56 (td, 1H, J = 7.8, 1.2 Hz), 7.50 (t, 1H, J = 7.8 Hz), 7.41 (dd, 1H, J = 2.7, 1.2 Hz), 7.22 (dd, 1H, J = 7.8, 2.7, 1.2 Hz), 6.07 (tt, 1H, J = 53.1, 4.2 Hz), 4.41 (tt, 2H, J = 12.1, 1.5 Hz); ^{13}C NMR ($CDCl_3$, 101 MHz, 295 K) δ 191.6, 158.0, 138.1, 130.6, 125.3, 122.0, 114.4 (tt, J = 249.9, 27.2 Hz), 112.9, 109.0 (tt, J = 249.9, 34.7 Hz), 65.2 (t, J = 29.8 Hz); ^{19}F NMR ($CDCl_3$, 376 MHz, 295 K) δ −124.8 (tq, 2F, J = 12.1, 4.3 Hz), −139.1 (dt, 2F, J = 53.1, 3.5 Hz); IR (neat, cm^{-1}) ν_{max} 2929, 1706, 1104.

3-benzyloxybenzaldehyde ***14*** [45]. K_2CO_3 (4.9 g, 35.47 mmol, 2.0

equiv) was added to a solution of 3-hydroxybenzaldehyde (2.17 g, 17.74 mmol, 1.0 equiv) in acetone (89 mL) with at 0 °C. After 5 min, the benzyl bromide (3.34 g, 19.51 mmol, 1.1 equiv) was added in the mixture. The solution was stirred for 1 night at rt. After concentrating the mixture *in vacuo*, the crude was dissolved with EtOAc, then the organic layer was washed with brine, dried over $MgSO_4$ and concentrated *in vacuo*. The crude was purified by chromatography on silica gel column (CHX/EtOAc, gradient 100:0 to 90:10) and concentrated under reduced pressure to afford the compound **14** as a white powder (2.48 g, 66% isolated yield). M. p. 60 °C; ^{1}H NMR ($CDCl_3$, 400 MHz, 295 K) δ 9.98 (s, 1H), 7.50–7.33 (m, 8H), 7.26 (m, 1H), 5.13 (s, 2H); ^{13}C NMR ($CDCl_3$, 100 MHz, 295 K) δ 192.2, 159.4, 137.9, 136.4, 130.2, 128.8 (2C), 128.3, 127.7 (2C), 123.8, 122.3, 113.3, 70.3.

(3-formylphenyl) N-ethyl-N-methylcarbamate **15** [31]. K_2CO_3 (6.79 g, 49.13 mmol, 3.0 equiv) was added to a solution of 3-hydroxybenzaldehyde (2.0 g, 16.38 mmol, 1.0 eq) in DMF (70 mL) at 0 °C. After 5 min, the ethylmethylcarbamic chloride (2.7 mL, 24.57 mmol, 1.5 equiv) was added to the mixture. The solution was then stirred for 2 h at 70 °C. After concentrating the mixture *in vacuo*, the crude product was dissolved with EtOAc, then the organic layer was washed with brine, dried over $MgSO_4$ and concentrated *in vacuo*. The crude product was purified by chromatography on silica gel column (CHX/EtOAc, gradient 100:0 to 70:30) and concentrated under reduced pressure to afford the compound **15** as a yellowish oil (2.96 g, 87% isolated yield). ^{1}H NMR (DMSO, 400 MHz, 363 K) δ 10.02 (s, 1H), 7.76 (td, 1H, J = 7.8, 1.2 Hz), 7.65 (dd, 1H, J = 2.4, 1.2, 0.4 Hz), 7.61 (dd, 1H, J = 7.8, 0.4 Hz), 7.46 (dd, 1H, J = 7.8, 2.4, 1.2 Hz), 3.41 (q, 2H, J = 7.1 Hz), 3.00 (s, 3H), 1.19 (t, 3H, J = 7.1 Hz); ^{13}C NMR (DMSO, 100 MHz, 363 K) δ 191.6, 152.8, 151.6, 137.2, 129.6, 127.2, 125.6, 121.4, 43.2, 33.3, 12.0.

5.1.3. General procedure for the synthesis of compounds (2, 7, 16)

Procedure A. To a stirred solution of amine (1.0 equiv) in MeOH, was added aldehyde (1.1 equiv) with few drops of acetic acid was stirred at rt for 1 night. $NaBH_4$ (3.0 equiv) was added and the solution was stirred at rt for 5 h. The solvent was removed *in vacuo*. The crude was purified by flash chromatography on silica gel column (DCM/MeOH, gradient 100:0 to 80:20), and concentrated under reduced pressure to afford amine compound.

2-(6-fluoro-1H-indol-3-yl*)-N-[[3-(2,2,3,3-tetrafluoropropoxy) phenyl]methyl]ethanamine* **2**. Following *procedure A* from **11** (185 mg, 1.04 mmol) and **13**, we obtained **2** as a brown oil (21 mg, 5% isolated yield). ^{1}H NMR (MeOD, 400 MHz, 295 K) δ 7.43 (dd, 1H, J = 8.7, 5.4 Hz), 7.24 (t, 1H, J = 8.0 Hz), 7.03 (s, 1H), 7.02 (dd, 1H, J = 10.0, 2.4 Hz), 6.93 (m, 1H, H_8), 6.92 (d, 1H, J = 1.6 Hz), 6.88 (m, 1H), 6.76 (dd, 1H, J = 9.8, 8.7, 2.4 Hz), 6.31 (tt, 1H, J = 52.8, 5.4 Hz), 4.38 (tt, 2H, J = 12.4, 1.6 Hz), 3.75 (s, 2H), 2.98–2.92 (m, 2H), 2.91–2.85 (m, 2H); ^{13}C NMR (MeOD, 101 MHz, 295 K) δ 161.2 (d, J = 253.2 Hz), 159.2, 142.4, 138.1 (d, J = 12.1 Hz), 130.7, 125.4, 123.9 (d, J = 3.0 Hz), 123.3, 120.1 (d, J = 10.1 Hz), 116.2 (tt, J = 248.0, 26.6 Hz), 115.6, 114.6, 113.6, 110.0 (tt, J = 247.5, 33.1 Hz), 108.0 (d, J = 24.7 Hz), 98.2 (d, J = 25.8 Hz), 66.3 (t, J = 29.4 Hz), 53.9, 50.1, 26.0; ^{19}F NMR (MeOH, 376 MHz, 295 K) δ −124.6 (td, 1F, J = 9.9, 5.4 Hz), −127.4–127.5 (m, 2F), −141.6 (dt, 2F, J = 52.8, 4.8 Hz); MS m/z $[M+H]^+$ 399.52; HRMS/ESI m/z calcd. For $C_{20}H_{20}F_5N_2O$ $[M+H]^+$ 399.1496, found 399.1502; IR (neat, cm^{-1}) ν_{max} 3425, 1104.

N-[(3-benzyloxyphenyl)methyl]-2-(6-fluoro-1H-indol-3-yl*)ethanamine* ***16***. Following *procedure A* with **11** (458 mg, 2.57 mmol) and **14**, we obtained **16** as a brown powder (265 mg, 24% isolated yield). M. p. 128 °C; ^{1}H NMR (MeOD, 400 MHz, 295 K) δ 7.49 (dd, 1H, J = 8.6, 5.3 Hz), 7.42 (d, 2H, J = 7.5 Hz), 7.34 (t, 2H, J = 7.5 Hz), 7.33 (d, 1H, J = 8.0 Hz), 7.28 (t, 1H, J = 7.5 Hz), 7.15 (s, 1H), 7.13 (t, 1H, J = 2.0 Hz), 7.07 (dd, 1H, J = 9.6, 2.4 Hz), 7.05–7.02 (m, 2H), 6.82 (dd, 1H, J = 9.6, 8.6, 2.4 Hz), 5.09 (s, 2H), 4.14 (s, 2H), 3.25 (t, 2H, J = 7.5 Hz), 3.14 (t, 2H, J = 7.5 Hz); ^{13}C NMR (MeOD, 100 MHz, 295 K) δ 161.3 (d, J = 235.6 Hz), 160.6, 138.3, 138.2 (d, J = 12.6 Hz), 134.4, 131.4, 129.5 (2C), 129.0, 128.6 (2C), 124.9, 124.7 (d, J = 3.4 Hz), 123.1, 119.9 (d, J = 10.3 Hz), 117.3, 116.9, 110.7, 108.5 (d, J = 24.9 Hz), 98.4 (d, J = 26.0 Hz), 71.0, 52.2, 48.7, 23.4; ^{19}F NMR (MeOD, 374 MHz, 295 K) δ −121.0 (td, J = 9.6, 5.3 Hz); MS: m/z $[M+H]^+$ 375.51; HRMS/ESI: m/z calcd. For $C_{24}H_{24}FN_2O$ $[M+H]^+$ 375.1873, found 375.1873; IR (neat, cm^{-1}) ν_{max} 3432.

3-[[2-(6-fluoro-1H-indol-3-yl*)ethylamino]methyl]phenyl N-ethyl-N-methylcarbamate* **7**. Following *procedure A* with **11** (491 mg, 2.76 mmol) and **15**, we obtained **7** as a brown oil (211 mg, 21% isolated yield). ^{1}H NMR (DMSO, 400 MHz, 363 K) δ 10.60 (s, 1H), 7.48 (dd, 1H, J = 8.7, 5.4 Hz), 7.28 (t, 1H, J = 7.7 Hz), 7.14 (d, 1H, J = 7.7 Hz), 7.11–7.05 (m, 3H), 6.96 (dd, 1H, J = 7.7, 2.4 Hz), 6.79 (dd, 1H, J = 10.0, 8.7, 2.4 Hz), 3.78 (s, 2H), 3.39 (q, 2H, J = 7.1 Hz), 2.97 (s, 3H), 2.86 (m, 4H), 1.17 (t, 3H, J = 7.1 Hz); ^{13}C NMR (DMSO, 100 MHz, 363 K) δ 158.5 (d, J = 232.9 Hz), 153.2, 151.1, 142.1, 135.8 (d, J = 12.6 Hz), 128.2, 123.9, 123.8, 122.5 (d, J = 2.1 Hz), 120.4, 119.2, 118.7 (d, J = 10.6 Hz), 122.7, 106.0 (d, J = 24.7 Hz), 96.7 (d, J = 24.9 Hz), 52.0, 49.0, 43.0, 33.2, 25.0, 12.1; ^{19}F NMR (DMSO, 374 MHz, 295 K) δ −124.5 (td, J = 9.9 Hz, J = 5.4 Hz); MS: m/z $[M+H]^+$ 370.53; HRMS/ESI: m/z calcd. For $C_{21}H_{25}FN_3O_2$ $[M+H]^+$ 370.1931, found 370.1929; IR (neat, cm^{-1}) ν_{max} 3425, 1706, 1168.

5.1.4. Synthesis of compound 6

3-[[2-(6-fluoro-1H-indol-3-yl*)ethylamino]methyl]phenol* **6**. To a stirred solution of **16** (527 mg, 1.41 mmol, 1.0 equiv) in MeOH (120 mL) was charged Pd/C 10% (150 mg, 10 mol%) and the mixture was stirred for 60 h under H_2 at room temperature. The mixture was filtered through a pad of Celite and evaporated. The crude was purified by flash chromatography on silica gel column (DCM/MeOH, gradient 100:0 to 95:5) and to afford the compound **6** as a brown powder (149 mg, 37% isolated yield). M. p. 70–80 °C; ^{1}H NMR (MeOD, 400 MHz, 295 K) δ 7.49 (dd, 1H, J = 8.7, 5.2 Hz), 7.21 (t, 1H, J = 8.0 Hz), 7.12 (s, 1H), 7.06 (dd, 1H, J = 10.0, 2.3 Hz), 6.89–6.85 (m, 2H), 6.84–6.78 (m, 2H), 4.00 (s, 2H), 3.17 (t, 2H, J = 6.8 Hz), 3.09 (t, 2H, J = 6.8 Hz); ^{13}C NMR (MeOD, 100 MHz, 295 K) δ 161.2 (d, J = 235.3 Hz), 159.1, 138.1 (d, J = 12.5 Hz), 136.0, 131.1, 125.0, 124.4 (d, J = 3.3 Hz), 121.4, 120.0 (d, J = 10.3 Hz), 117.3, 116.8, 111.4, 108.4 (d, J = 24.9 Hz), 98.3 (d, J = 26.0 Hz), 52.7, 49.0, 23.9; ^{19}F NMR (MeOD, 374 MHz, 295 K) δ −124.1 (td, J = 9.8, 5.2 Hz); MS: m/z $[M+H]^+$ 285.48; HRMS/ESI: m/z calcd. For $C_{17}H_{18}FN_2O$ $[M+H]^+$ 285.1403, found 285.1405. IR (neat, cm^{-1}) ν_{max} 3427.

5.1.5. General procedure for the preparation of fumarate salts (17–18)

Procedure B. To a stirred solution of basic compound (1.0 equiv) in iPrOH was added fumaric acid (0.95 equiv). The solution was refluxed for 1 h. The mixture was then concentrated *in vacuo*. The residue was triturated in Et_2O and then filtrated to yield the fumarate salt.

3-[[2-(6-fluoro-1H-indol-3-yl*)ethylamino]methyl]phenol fumaric acid salt* ***17***. Following *procedure B* with compound **6** (240 mg, 0.84 mmol), we obtained compound **17**, as a brown yellow powder (212 mg, 63 yield). M. p. > 250 °C; ^{1}H NMR (MeOD, 400 MHz, 295 K) δ 7.48 (dd, 1H, J = 8.7, 5.4 Hz), 7.25 (t, 1H, J = 8.1 Hz), 7.15 (s, 1H), 7.06 (dd, 1H, J = 9.9, 2.3 Hz), 6.93–6.89 (m, 2H), 6.88–6.79 (m, 2H), 6.70 (s, 2H), 4.13 (s, 2H), 3.28 (t, 2H, J = 6.6 Hz), 3.14 (t, 2H, J = 6.6 Hz); ^{13}C NMR (MeOD, 101 MHz, 295 K) δ 171.3 (2C), 161.3 (d, J = 235.6 Hz), 159.4, 138.2 (d, J = 12.6 Hz), 136.2 (2C), 133.9, 131.4, 124.8, 124.7 (d, J = 3.6 Hz), 121.6, 119.9 (d, J = 10.3 Hz), 117.7, 117.5, 110.6, 108.5 (d, J = 24.9 Hz), 98.5 (d, J = 26.0 Hz), 52.1, 48.7, 23.2; ^{19}F NMR (MeOD, 376 MHz, 295 K) δ −124.0 (td, J = 9.9, 5.4 Hz); MS m/z $[M + H-C_4H_4O_4]^+$ 285.50; HRMS/ESI m/z calcd. For $C_{17}H_{18}FN_2O$ $[M+H]^+$ 285.1403, found 285.1404; IR (neat, cm^{-1}) ν_{max} 3358, 3047,

1693, 1593, 1458, 1278; RX (ORTEP) Crystal size: 0.62 × 0.29 × 0.19 mm. Formula $C_{21}H_{21}FN_2O_5$, molecular weight 400.40, crystal system monoclinic, space group *C2/C*, $a = 20.3537$ (16) Å, $b = 13.9674$ (16) Å, $c = 14.8582$ (14) Å, $\alpha = 90°$, $\beta = 113.160$ (4)°, $\gamma = 90°$, $V = 3883.6$ (7) Å^3, $Z = 8$, calculated density = 1.370 g/cm^3, $\mu = 0.105$ mm^{-1}, $R_{int} = 0.137$, R [$F^2 > 2s$ (F^2)] = 0.057, w*R* (F^2) = 0.164, $S = 1.03$.

3-[[2-(6-fluoro-1H-indol-3-yl)*ethylamino]methyl]phenyl N-ethyl-N-methylcarbamate fumaric acid salt* ***18***. Following *procedure B* with compound **7** (360 mg, 0.97 mmol), we obtained compound **18**, as a beige powder (345 mg, 73% yield). M. p. > 250 °C; ^{1}H NMR (MeOD, 400 MHz, 295 K) δ 7.50 (dd, 1H, J = 8.7, 5.1 Hz), 7.47 (t, 1H, J = 7.9 Hz), 7.33 (dt, 1H, J = 7.9, 1.2 Hz), 7.24 (t, 1H, J = 2.2 Hz), 7.19 (dd, 1H, J = 7.9, 2.2, 1.2 Hz), 7.16 (s, 1H), 7.06 (dd, 1H, J = 9.8, 2.3, 0.5 Hz), 6.83 (dd, 1H, J = 9.8, 8.7, 2.3 Hz), 6.69 (s, 2H), 4.22 (s, 2H), 3.51 (q, 1H, J = 7.2 Hz, rota A), 3.41 (q, 1H, J = 7.2 Hz, rota B), 3.33−3.31 (m, 2H), 3.15 (t, 2H, J = 7.8 Hz), 3.11 (s, 1.5H, rota A), 2.99 (s, 1.5H, rota B), 1.27 (t, 1.5H, J = 7.2 Hz, rota A), 1.19 (t, 1.5H, J = 7.2 Hz, rota B); ^{13}C NMR (MeOD, 101 MHz, 295 K) δ 172.0 (2C), 161.3 (d, J = 235.7 Hz), 156.1, 153.3, 138.2 (d, J = 12.5 Hz), 136.4 (2C), 134.3, 131.3, 127.9, 124.9, 124.7 (d, J = 3.4 Hz), 124.5 (d, J = 7.4 Hz), 124.1, 119.9 (d, J = 10.3 Hz), 110.4, 108.5 (d, J = 24.9 Hz), 98.4 (d, J = 25.9 Hz), 51.7, 49.0, 45.3 (rota A), 45.2 (rota B), 34.6 (rota A), 34.3(rota B), 23.3, 13.4 (rota A), 12.6 (rota B); ^{19}F NMR (MeOD, 376 MHz) δ −124.0 (td, J = 9.8 Hz, J = 5.4 Hz); MS *m/z* [M + H−$C_4H_4O_4$]$^+$ 370.58; HRMS/ESI *m/z* calcd. For $C_{21}H_{25}FN_3O_2$ [M+H]$^+$ 370.1931, found 370.1932; IR (neat, cm^{-1}) ν_{max} 2976, 1699, 1240, 1165.

5.2. In vitro tests of hAChE and hBuChE inhibitory activity

The inhibitory capacity of compounds on AChE biological activity was evaluated through the use of the spectrometric method of Ellman [36]. Acetylthiocholine iodide and 5,5-dithiobis-(2-nitrobenzoic) acid (DTNB) were purchased from Sigma Aldrich. AChE from human erythrocytes (buffered aqueous solution, ≥ 500 units/mg protein (BCA), Sigma Aldrich, St. Louis, MO, USA) was diluted in 20 mM HEPES buffer pH 8, 0.1% Triton X-100 such as to have enzyme solution with 0.25 unit/mL enzyme activity. In the procedure, 100 μL of 0.3 mM DTNB dissolved in a phosphate buffer with pH 7.4 were added into the 96-well plates followed by 50 μL of the test compound solution and 50 μL of enzyme (0.05 U final). After 5 min of pre-incubation at 25 °C, the reaction was then initiated by the injection of 50 μL of 1 mM acetylthiocholine iodide solution. The hydrolysis of acetylthiocholine was monitored by the formation of yellow 5-thio-2-nitrobenzoate anion as the result of the reaction of DTNB with thiocholine, released by the enzymatic hydrolysis of acetylthiocholine, at a wavelength of 412 nm using a 96-well microplate plate reader (BioTek, Synergy 2). Test compounds were dissolved in analytical grade DMSO. Donepezil was used as a reference standard.

Inhibitory capacity of compounds on human butyrylcholinesterase (*h*BuCHE) biological activity was evaluated through the use of the spectrometric method of Ellman [36]. Butyrylthiocholine iodide and DTNB were purchased from Sigma Aldrich. BuChE from human was diluted in 0.1 M phosphate buffer (pH 7.4) to have enzyme solution with 1 unit/mL enzyme activity. In the procedure, 100 μL of 0.3 mM DTNB dissolved in phosphate buffer pH 7.4 were added into the 96 wells plate followed by 50 μL of test compound solution and 50 μL of enzyme (0.20 U final). After 5 min of pre-incubation at 25 °C, the reaction was then initiated by the injection of 50 μL of 1 mM butyrylthiocholine iodide solution. The hydrolysis of butyrylthiocholine was monitored by the formation of yellow 5-thio-2-nitrobenzoate anion as the result of the reaction of DTNB with thiocholine, released by the enzymatic hydrolysis of butyrylthiocholine, at a wavelength of 412 nm using a 96-well microplate plate reader (BioTek, Synergy 2). Test compounds were dissolved at 5 × 10^{-3} M in analytical grade DMSO. Tacrine was used as a reference standard. The rate of absorbance increase at 412 nm was followed every minute for 10 min. Assays were performed with a blank containing all components except inhibitor compound.

The reaction slopes were compared and the percent inhibition due to the presence of test compounds was calculated by the following expression: $((v_0-v_i)/v_0)$ x 100 where v_i is the rate calculated in the presence of inhibitor and v_0 is the enzyme activity. First screening of *h*BuChE activity was carried out at a 10^{-5} M concentration of compounds under study. For the compounds with significant inhibition (≥65%), IC_{50} values were determined graphically by plotting the % inhibition versus the logarithm of six inhibitor concentrations in the assay solution using the GraphPad Prism 6 software.

5.3. Kinetic study for eqBuChE inhibition

To try to clarify the mechanism of action **18**, reciprocal plots of 1/velocity vs. 1/[substrate] were constructed at different concentrations of the substrate butyrylthiocholine iodide (0.1−1 mM) by using the spectrometric method by Ellman et al. [36]. Four concentrations of **18** were selected for the studies: 10 nM, 50 nM, 100 nM and 500 nM for the kinetic analysis of *eq*BuChE inhibition. The plots were assessed by a weighted least squares analysis that assumed the variance of velocity (ν) to be a constant percentage of ν for the entire dataset. Slopes of these reciprocal plots were then plotted against the concentration of **18** in a weighted analysis.

5.4. Pharmacological characterization of drugs on human 5-HT$_6$R

Drugs were evaluated through their possibility to compete for the binding of [^{3}H]-LSD on membranes of HEK-293 cells transiently expressing the human 5-HT$_6$ receptors (ref. RBHS6M, PerkinElmer). In brief, 4 μg of proteins were incubated at 37 °C for 60 min in duplicate in the absence or the presence of 10^{-6} or 10^{-8} M of each drug (SB271046 was used as a reference standard) and 2.5 nM [^{3}H]-LSD (ref. NET638250UC, PerkinElmer), in 25 mM Tris-HCl buffer (pH 7.4) supplemented with 0.5 mM EDTA. At the end of the incubation, the homogenates were then filtered through Whatman GF/C filters and washed five times with ice-cold 25 mM Tris-HCl buffer. Non-specific binding was evaluated in the presence of 100 μM serotonin. Radioactivity associated to proteins was then quantified and expressed as the percentage of inhibition of the drugs under study.

For some of these compounds, affinity constants were calculated from five-point inhibition curves using the GraphPad Prism 6 software and expressed as Ki ± SD.

5.5. Determination of cAMP production

COS-7 cells were grown in Dulbecco's modified Eagle medium (DMEM) supplemented with 10% dialyzed fetal calf serum (dFCS) and antibiotics. Cells were transiently transfected by electroporation with plasmids encoding HA-tagged 5-HT$_6$R (70 ng/10^6 cells or 300 ng/10^6 cells), then seeded in 96-well plates (16,000 cells/well).

Blockade of the 5-HT$_6$R-induced cAMP production: 24 h after transfection, cells were exposed to the indicated concentrations of 5-HT$_6$R ligands at 37 °C in 50 μL of HBS. After 7 min, 5-HT (5.10^{-7} M final concentration) in the presence of RO-20-1724 (0.1 mM final concentration), in 50 μL HBS, was added to the wells. After 10 min at 37 °C, cells were then lysed by addition of 100 μL of Triton-X100 (0.1%).

Quantification of cAMP production was performed by HTRF® by

using the cAMP Dynamic kit (Cisbio Bioassays) according to the manufacturer's instructions.

5.6. Parallel artificial membrane permeability

The PAMPA-BBB experiments were conducted using the Pampa Explorer Kit (Pion Inc., Billerica, MA, USA) according to the protocol provided by the manufacturer. Briefly, the donecopride fumarate solution (20 mM in DMSO) was diluted in Prisma HT buffer (pH 7.4; pION) to 100 μM; 200 μL this solution (n = 6) was added to the donor plate (P/N 110,243). Five microliters BBB-1 Lipid (P/N 110,672) was used to coat the membrane filter of the acceptor plate (P/N 110,243). Two hundred microliters Brain Sink Buffer (P/N 110,674) was added to each well of the acceptor plate. The PAMPA sandwich was assembled and allowed to incubate at room temperature for 4 h without stirring. The sandwich was then separated, and the UV−visible spectra were measured for both the donor and receiver wells with the microplate reader (Tecan Infinite M200). The −logPe and Pe (PAMPA effective permeability coefficient) were calculated by the PAMPA Explorer software version 3.7 (pION) for studied compounds. Corticosterone (−logPe = 4.80, Pe = 15.77 × 10^{-6} cm/s) and theophylline (-log Pe = 6.35, Pe = 0.45 × 10^{-6} cm/s) were used as positive and negative references, respectively.

5.7. BuChE-dependent decarbamoylation

Solutions of compound **18** were prepared in a PBS buffer (pH 7.4). BuChE from *Electrophorus electricus* (buffered aqueous solution, ≥ 500 units/mg protein (BCA), Sigma Aldrich) was diluted in PBS buffer pH 7.4, to reach enzyme activity at 250 unit/mL. Solution was prepared by addition of 250 μL of the abovementioned enzyme stock solution to 5 μL of solution of compounds 19 or 20 at 255 μM. The mixture was stirred during 24 h at room temperature. The mixture was extracted by 300 μL of EtOAc, and 250 μL of the organic layer was reduced by nitrogen flow. The crude product was submerged in 50 μL of ACN, then analyzed by HPLC.

The HPLC analyses were performed using an Agilent (Agilent technologies, Santa Clara, CA, USA) binary pump 1290, an autosampler 1290 and a diode array UV detector 1260. A reversed phase column C18 (Restek® Ultra, 5 μm, 2.1 × 50 mm) has been used for all components. The mobile phase was always composed of a mixture of (A) water (0.1% formic acid) and (B) acetonitrile using a gradient mode (Table 5). Injection volumes was 6 μL, flow rate, 0.6 mL/min and total analysis time 3.2 min (Table 6).

5.8. Molecular docking and molecular dynamic simulation

The initial model of compound **18** was built from solved X-ray structure of **17** and its protonation state at pH 7.4 was predicted using standard tools of the ChemAxon Package [38]. The majority microspecie protonated on amine nitrogen at this pH was used for docking studies.

The crystallographic coordinates of human butyrylcholinesterase were obtained from X-ray structure of human butyrylcholinesterase in complex with (*S*)−*N*-(1-((2-cycloheptylethyl) amino)-3-(1*H*-indol-3-yl)-1-oxopropan-2-yl)-*N*,*N*-dimethylbutan-1-aminium (PDB ID 6QAB, a structure refined to 2.49 Å with an R free factor of 23.6%) [46]. The BuChE amino acid protonation state was check before the docking study using the ProPKA software and the proposed protonation for Glu 197 was applied. The docking of the compound into the BuChE binding site was carried out with the GOLD program (v5.7.2) using the default parameters [47,48]. This program applies a genetic algorithm to explore conformational spaces and ligand binding modes. To evaluate the proposed ligand positions, the ChemPLP fitness function was applied. The binding site in the BuChE model was defined as a 7 Å sphere from the co-crystallized ligand. The Ser198 side chain was kept flexible and a hydrogen bond constraint between Ser198 side chain and carbonyl oxygen of ligand was used during the docking.

Next, the stability of the selected binding poses was assessed using two unbiased molecular dynamics simulations of 50 ns each. All the simulations were performed using NAMD 2.12 [49]. The all-atom CHARMM 36 m forcefield [50,51] was used for the protein and CGENFF [52] for **18**. The CHARMM-GUI server [53] was used to prepare the starting systems. Each system was solvated using the TIP3P explicit water model [54] within a rectangular box; the box size ensured that the simulated complex was at a minimum distance of 10 Å from the edge. 0.15 M of NaCl was added to neutralize the total charge of the system. Periodic boundary conditions were applied to the systems using the IMAGE algorithm. van der Waals interactions were truncated using a force switching function between 10 and 12 Å and the Particle Mesh Ewald (PME) [55] was used to calculate long-range electrostatic interactions. The SHAKE algorithm was applied to restrain all bonds involving hydrogen atoms.

The systems underwent energy minimization in 10,000 steps. Next, the minimized systems were heated to 300 K and the dynamics were temperature-equilibrated during 50 ps *via* heating reassignment under NVT conditions. Finally, the systems ran freely for 50 ns under NPT conditions with a 2 fs time step. Langevin dynamics with a damping coefficient of 1 ps^{-1} were used to maintain the system temperature and the Nosé-Hover Langevin piston was used to maintain a 1 atm pressure. Production trajectories were saved every 10 ps and subsequent analyses were performed using the CHARMM program version c40b2 [56] and κ clustering was carried out by "Multiscale Modeling Tools for Structural Biology" software.

5.9. In vivo biological studies animals

5.9.1. Animals

Adult male NMRI mice (3 months old, weighing 35−40 g) from Janvier labs (Le Genest-Saint-Isle, France) were used to perform experiments. Mice were housed by ten in standard polycarbonate cages in standard controlled conditions (22 ± 2 °C, 55 ± 10% humidity) with a reversed 12 h light/dark cycle (light on at 7 p.m.). Food and water were available ad libitum in the home cage. All experiments were conducted (between 9 a.m. and 3 p.m.) during the active−dark phase of the cycle and were in agreement with the European Directives and French law on animal experimentation (personal authorization n° 14−17 for MB and 14−60 for TF).

Table 5
Gradient conditions.

Method		Rivastigmine			18		
Time (min)		0	0.8	1.9	0	3.0	3.2
Solvent (%)	A	95	90	30	90	30	30
	B	5	10	70	10	70	70

Table 6
HPLC conditions.

Compound	Carbamate	Rivastigmine	18
	Phenol	3-[(1*S*)-1-(dimethylamino)ethyl]phenol	17
Retention time (min)	Carbamate	1.51	1.81
	Phenol	2.15	1.73
Wavelength (nm)		265	280

5.9.2. CNS-activity and acute toxicity test

Behavioral and neurological changes induced by graded doses (1, 10, 100 mg/kg) of the tested derivatives **17** and **18** were evaluated in mice, in groups of four, by a standardized observation technique at different times (30 min, 3 and 24 h) after intraperitoneal administration [57]. Major changes of behavioral data (for example, hypo- or hyperactivity, ataxia, tremors, convulsion, etc.) were noted in comparison to the control group. The approximate LD_{50} of the compounds were also calculated through the quantification of mortality after 24 h. Amphetamine (2 mg/kg) and chlorpromazine (10 mg/kg) were used as the stimulant and depressive references, respectively.

5.9.3. Locomotor activity

The locomotion of mice was measured using an actimeter (Imetronic®) through infrared detection. Eight individual removable polycarbonate cages (21 cm length, 7c m wide and 12 cm high), in which each mouse was placed, were used in the actimeter. Locomotor activity was measured by recording the number of interruptions of beams of the red light over a period of 30 min through a recording system attached to the actimeter. Compounds **17** and **18** were tested at 1, 3 and 10 mg/kg. Chlorpromazine (3 mg/kg) were used as depressive reference [58].

5.9.4. Spatial working memory

The antiamnesic activity of the tested compounds was evaluated by a reversal of deficit on spontaneous alternation behavior in the Y maze test [59]. Deficits were pharmacologically induced either by scopolamine (SCOP, 0.5 mg/kg) or dizocilpine (MK801, 0.1 mg/kg). The Y maze made of grey plastic consisted of three equally-spaced arms (21-cm long, 7-cm wide with walls 15-cm high). The mouse was placed at the end of one of the arms and allowed to move freely through the maze during a 5 min session, while the sequence of arm entries was recorded by an observer. An arm entry was scored when all four feet crossed into the arm. An alternation was defined as entries into all three arms on a consecutive occasion. The number of possible alternations is thus the total number of arm entries minus two; the percentage of alternation was calculated as (actual alternation/possible alternation) 100. Compounds **17** and **18** were tested at 10 mg/kg.

5.9.5. Pharmacological treatments

Amphetamine (+)-α-Methylphenethylamine hemisulfate, chlorpromazine hydrochloride, MK801 hydrogen maleate and scopolamine hydrobromide were purchased from Sigma (France). All pharmacological compounds were dissolved in NaCl 0.9%, used as vehicle. Besides, all were administered IP 30 min before tests, except for scopolamine and MK801, which were subcutaneously administered 20 min before spontaneous alternation test.

5.9.6. Statistical analysis

Results were expressed as mean ± SD and were analyzed by one-way analysis of variance (ANOVA), with Statview® software. In case of significance, a SNK (Student-Newman-Keuls) post hoc test was realized. Additionally, for the spontaneous alternation test, the percentage of alternation was compared to a theoretical 50% value (random alternation) by a univariate *t-test*. Differences were considered as statistically significant if the p value was strictly under 0.05.

Author contributions

Conceptualization, T.F., S.C., M.B., P.D. and C.R.; methodology, F.-X.T., J.L., B.H., A.D., M.S., S.C. and J.S.d.O.S.; software, J.S.d.O.S.; validation, T.F., S.C., M.B., P.D. and C.R.; writing—original draft preparation, F.-X.T., P.D. and C.R.; writing—review and editing, F.-X.T., T.F., S.C., M.B., P.D. and C.R.; funding acquisition, S.C., P.D. and C.R.

Declaration of competing interest

The authors declare that they have no known competing financial interests or personal relationships that could have appeared to influence the work reported in this paper.

Acknowledgment

This work was supported by funding from the Fondation Vaincre Alzheimer (#FR-15072) and the Fondation Plan Alzheimer (AAP2015 Project TRIAD 016). The authors gratefully acknowledge the Conseil Régional de Normandie, as well as the European Community (FEDER) for their contribution to the CERMN's analytical platform. European COST action CA15135 (Multi-Target Paradigm for Innovative Ligand Identification in the Drug Discovery Process, MuTaLig) supports this article. Part of this work was performed using computing resources of CRIANN (Normandy, France) as well as the European Community (FEDER) for the molecular modeling software. We thank Oksana Lockridge at Eppley Institute University of Nebraska Medical Center Omaha, for providing us human BuChE.

Appendix A. Supplementary data

Supplementary data to this article can be found online at https://doi.org/10.1016/j.ejmech.2020.113059.

References

[1] M.G. Savelieff, G. Nam, J. Kang, H.J. Lee, M. Lee, M.H. Lim, Development of multifunctional molecules as potential therapeutic candidates for Alzheimer's disease, Parkinson's disease, and amyotrophic lateral sclerosis in the last decade, Chem. Rev. 119 (2019) 1221–1322, https://doi.org/10.1021/acs.chemrev.8b00138.
[2] J. Birks, J. Grimley Evans, V. Iakovidou, M. Tsolaki, F.E. Holt, Rivastigmine for Alzheimer's disease, Cochrane Database Syst. Rev. 15 (2009), CD001191, https://doi.org/10.1002/14651858.CD001191.pub2.
[3] L.A. Craig, N.S. Hong, R.J. McDonald, Revisiting the cholinergic hypothesis in the development of Alzheimer's disease, Neurosci. Biobehav. Rev. 35 (2011) 1397–1409, https://doi.org/10.1016/j.neubiorev.2011.03.001.
[4] E. Giacobini, Cholinergic function and Alzheimer's disease, Int. J. Geriatr. Psychiatr. 18 (2003) S1–S5, https://doi.org/10.1002/gps.935.
[5] N.H. Greig, T. Utsuki, D.K. Ingram, Y. Wang, G. Pepeu, C. Scali, Q.-S. Yu, J. Mamczarz, H.W. Holloway, T. Giordano, D. Chen, K. Furukawa, K. Sambamurti, A. Brossi, D.K. Lahiri, Selective butyrylcholinesterase inhibition elevates brain acetylcholine, augments learning and lowers Alzheimer β-

amyloid peptide in rodent, Proc. Natl. Acad. Sci. Unit. States Am. 102 (2005) 17213–17218, https://doi.org/10.1073/pnas.0508575102.
[6] P. Sharma, P. Srivastava, A. Seth, P.N. Tripathi, A.G. Banerjee, S.K. Shrivastava, Comprehensive review of mechanisms of pathogenesis involved in Alzheimer's disease and potential therapeutic strategies, Prog. Neurobiol. 174 (2019) 53–89, https://doi.org/10.1016/j.pneurobio.2018.12.006.
[7] L. Jing, G. Wu, D. Kang, Z. Zhou, Y. Song, X. Liu, P. Zhan, Contemporary medicinal-chemistry strategies for the discovery of selective butyrylcholinesterase inhibitors, Drug Discov. Today 24 (2019) 629–635, https://doi.org/10.1016/j.drudis.2018.11.012.
[8] M. Hoffmann, C. Stiller, E. Endres, M. Scheiner, S. Gunesch, C. Sotriffer, T. Maurice, M. Decker, Highly selective butyrylcholinesterase inhibitors with tunable duration of action by chemical modification of transferable carbamate units exhibit pronounced neuroprotective effect in an Alzheimer's disease mouse model, J. Med. Chem. 62 (2019) 9116–9140, https://doi.org/10.1021/acs.jmedchem.9b01012.
[9] Z. Cai, Monoamine oxidase inhibitors: promising therapeutic agents for Alzheimer's disease (Review), Mol. Med. Rep. 9 (2014) 1533–1541, https://doi.org/10.3892/mmr.2014.2040.
[10] J. Lalut, D. Karila, P. Dallemagne, C. Rochais, Modulating 5-HT 4 and 5-HT 6 receptors in Alzheimer's disease treatment, Future Med. Chem. 9 (2017) 781–795, https://doi.org/10.4155/fmc-2017-0031.
[11] S. Claeysen, J. Bockaert, P. Giannoni, Serotonin: a new hope in Alzheimer's disease? ACS Chem. Neurosci. 6 (2015) 940–943, https://doi.org/10.1021/acschemneuro.5b00135.
[12] M.J. Ramírez, 5-HT6 receptors and Alzheimer's disease, Alzheimer's Res. Ther. 5 (2013) 15, https://doi.org/10.1186/alzrt169.
[13] J. Godyń, J. Jończyk, D. Panek, B. Malawska, Therapeutic strategies for Alzheimer's disease in clinical trials, Pharmacol. Rep. 68 (2016) 127–138, https://doi.org/10.1016/j.pharep.2015.07.006.
[14] D. Karila, T. Freret, V. Bouet, M. Boulouard, P. Dallemagne, C. Rochais, Therapeutic potential of 5-HT 6 receptor agonists, J. Med. Chem. 58 (2015) 7901–7912, https://doi.org/10.1021/acs.jmedchem.5b00179.
[15] B. Benhamú, M. Martín-Fontecha, H. Vázquez-Villa, L. Pardo, M.L. López-Rodríguez, Serotonin 5-HT6 receptor antagonists for the treatment of cognitive deficiency in Alzheimer's disease, J. Med. Chem. 57 (2014) 7160–7181, https://doi.org/10.1021/jm5003952.
[16] J. Arnt, B. Bang-Andersen, B. Grayson, F.P. Bymaster, M.P. Cohen, N.W. DeLapp, B. Giethlen, M. Kreilgaard, D.L. McKinzie, J.C. Neill, D.L. Nelson, S.M. Nielsen, M.N. Poulsen, J.M. Schaus, L.M. Witten, Lu AE58054, a 5-HT6 antagonist, reverses cognitive impairment induced by subchronic phencyclidine in a novel object recognition test in rats, Int. J. Neuropsychopharmacol. 13 (2010) 1021–1033, https://doi.org/10.1017/S1461145710000659.
[17] L.S. Schneider, Idalopirdine for Alzheimer's disease: written in the stars, Lancet Neurol. 13 (2014) 1063–1065, https://doi.org/10.1016/S1474-4422(14)70232-7.
[18] A. Atri, L. Frölich, C. Ballard, P.N. Tariot, J.L. Molinuevo, N. Boneva, K. Windfeld, L.L. Raket, J.L. Cummings, Effect of idalopirdine as adjunct to cholinesterase inhibitors on change in cognition in patients with Alzheimer disease, J. Am. Med. Assoc. 319 (2018) 130–142, https://doi.org/10.1001/jama.2017.20373.
[19] L. Frölich, A. Atri, C. Ballard, P.N. Tariot, J.L. Molinuevo, N. Boneva, M.A. Geist, L.L. Raket, J.L. Cummings, Open-label, multicenter, phase III extension study of Idalopirdine as adjunctive to Donepezil for the treatment of mild-moderate Alzheimer's disease, J. Alzheim. Dis. 67 (2019) 303–313, https://doi.org/10.3233/JAD-180595.
[20] C.F. Ferris, P. Kulkarni, J.R. Yee, M. Nedelman, I.E.M. de Jong, The serotonin receptor 6 antagonist idalopirdine and acetylcholinesterase inhibitor donepezil have synergistic effects on brain activity-a functional MRI study in the awake rat, Front. Pharmacol. 8 (2017) 279, https://doi.org/10.3389/fphar.2017.00279.
[21] A. Cavalli, M.-L. Bolognesi, A. Minarini, M. Rosini, V. Tumiatti, M. Recanatini, C. Melchiorre, Multi-target-directed ligands to combat neurodegenerative diseases, J. Med. Chem. 51 (2008) 347–372, https://doi.org/10.1021/jm7009364.
[22] C. Albertini, A. Salerno, P. de Sena Murteira Pinheiro, M.L. Bolognesi, From combinations to multitarget-directed ligands: a continuum in Alzheimer's disease polypharmacology, Med. Res. Rev. (2020) 1–28, https://doi.org/10.1002/med.21699.
[23] J. Lalut, C. Rochais, P. Dallemagne, Multiple ligands in neurodegenerative diseases. https://doi.org/10.1002/9783527674381.ch16, 2017, 477-508.
[24] C. Lecoutey, D. Hedou, T. Freret, P. Giannoni, F. Gaven, M. Since, V. Bouet, C. Ballandonne, S. Corvaisier, A. Malzert Freon, S. Mignani, T. Cresteil, M. Boulouard, S. Claeysen, C. Rochais, P. Dallemagne, Design of donecopride, a dual serotonin subtype 4 receptor agonist/acetylcholinesterase inhibitor with potential interest for Alzheimer's disease treatment, Proc. Natl. Acad. Sci. Unit. States Am. 111 (2014) E3825–E3830, https://doi.org/10.1073/pnas.1410315111.
[25] C. Rochais, C. Lecoutey, F. Gaven, P. Giannoni, K. Hamidouche, D. Hedou, E. Dubost, D. Genest, S. Yahiaoui, T. Freret, V. Bouet, F. Dauphin, J. Sopkova de Oliveira Santos, C. Ballandonne, S. Corvaisier, A. Malzert-Fréon, R. Legay, M. Boulouard, S. Claeysen, P. Dallemagne, J.S. De Oliveira Santos, C. Ballandonne, S. Corvaisier, A. Malzert-Fréon, R. Legay, M. Boulouard, S. Claeysen, P. Dallemagne, Novel multitarget-directed ligands (MTDLs) with acetylcholinesterase (AChE) inhibitory and serotonergic subtype 4 receptor (5-HT4R) agonist activities as potential agents against Alzheimer's disease: the design of Donecopride, J. Med. Chem. 58 (2015) 3172–3187, https://doi.org/10.1021/acs.jmedchem.5b00115.
[26] C. Rochais, C. Lecoutey, K. Hamidouche, P. Giannoni, F. Gaven, E. Cem, S. Mignani, K. Baranger, T. Freret, J. Bockaert, S. Rivera, M. Boulouard, P. Dallemagne, S. Claeysen, Donecopride, a Swiss army knife with potential against Alzheimer's disease, Br. J. Pharmacol. 177 (2020) 1988–2005, https://doi.org/10.1111/bph.14964.
[27] A. Więckowska, M. Kołaczkowski, A. Bucki, J. Godyń, M. Marcinkowska, K. Więckowski, P. Zaręba, A. Siwek, G. Kazek, M. Głuch-Lutwin, P. Mierzejewski, P. Bienkowski, H. Sienkiewicz-Jarosz, D. Knez, T. Wichur, S. Gobec, B. Malawska, Novel multi-target-directed ligands for Alzheimer's disease: combining cholinesterase inhibitors and 5-HT6 receptor antagonists. Design, synthesis and biological evaluation, Eur. J. Med. Chem. 124 (2016) 63–81, https://doi.org/10.1016/j.ejmech.2016.08.016.
[28] S. Yahiaoui, K. Hamidouche, C. Ballandonne, A. Davis, J.S. de Oliveira Santos, T. Freret, M. Boulouard, C. Rochais, P. Dallemagne, Design, synthesis, and pharmacological evaluation of multitarget-directed ligands with both serotonergic subtype 4 receptor (5-HT4R) partial agonist and 5-HT6R antagonist activities, as potential treatment of Alzheimer's disease, Eur. J. Med. Chem. 121 (2016) 283–293, https://doi.org/10.1016/j.ejmech.2016.05.048.
[29] B. Hatat, S. Yahiaoui, C. Lecoutey, A. Davis, T. Freret, M. Boulouard, S. Claeysen, C. Rochais, P. Dallemagne, A novel in vivo anti-amnesic agent, specially designed to express both acetylcholinesterase (AChE) inhibitory, serotonergic subtype 4 receptor (5-HT4R) agonist and serotonergic subtype 6 receptor (5-HT6R) inverse agonist activities, with a potential inter, Front. Aging Neurosci. 11 (2019) 148, https://doi.org/10.3389/fnagi.2019.00148.
[30] D.A. Rodríguez-Soacha, M. Scheiner, M. Decker, Multi-target-directed-ligands acting as enzyme inhibitors and receptor ligands, Eur. J. Med. Chem. 180 (2019) 690–706, https://doi.org/10.1016/j.ejmech.2019.07.040.
[31] F.-X. Toublet, C. Lecoutey, J. Lalut, B. Hatat, A. Davis, M. Since, S. Corvaisier, T. Freret, J. Sopkova de Oliveira Santos, S. Claeysen, M. Boulouard, P. Dallemagne, C. Rochais, Inhibiting acetylcholinesterase to activate pleiotropic prodrugs with therapeutic interest in Alzheimer's disease, Molecules 24 (2019) 2786, https://doi.org/10.3390/molecules24152786.
[32] M. Yogev-Falach, O. Bar-Am, T. Amit, O. Weinreb, M.B.H. Youdim, A multifunctional, neuroprotective drug, ladostigil (TV3326), regulates holo-APP translation and processing, Faseb. J. 20 (2006) 2177–2179, https://doi.org/10.1096/fj.05-4910fje.
[33] J. Reis, F. Cagide, M.E. Valencia, J. Teixeira, D. Bagetta, C. Pérez, E. Uriarte, P.J. Oliveira, F. Ortuso, S. Alcaro, M.I. Rodríguez-Franco, F. Borges, Multi-target-directed ligands for Alzheimer's disease: discovery of chromone-based monoamine oxidase/cholinesterase inhibitors, Eur. J. Med. Chem. 158 (2018) 781–800, https://doi.org/10.1016/j.ejmech.2018.07.056.
[34] H. Wang, H. Zhang, Reconsideration of anticholinesterase therapeutic strategies against Alzheimer's disease, ACS Chem. Neurosci. 10 (2019) 852–862, https://doi.org/10.1021/acschemneuro.8b00391.
[35] M.E. Muratore, C.A. Holloway, A.W. Pilling, R.I. Storer, G. Trevitt, D.J. Dixon, Enantioselective Bronsted acid-catalyzed N-acyliminium cyclization cascades, J. Am. Chem. Soc. 131 (2009) 10796–10797, https://doi.org/10.1021/ja9024885.
[36] G.L. Ellman, K.D. Courtney, V.J. Andres, R.M. Featherstone, A new and rapid colorimetric determination of acetylcholinesterase activity, Biochem. Pharmacol. 7 (1961) 88–95, https://doi.org/10.1016/0006-2952(61)90145-9.
[37] Q.-S. Yu, X. Zhu, H.W. Holloway, N.F. Whittaker, A. Brossi, N.H. Greig, Anticholinesterase activity of compounds related to Geneserine tautomers. N -Oxides and 1,2-Oxazines, J. Med. Chem. 45 (2002) 3684–3691, https://doi.org/10.1021/jm010491d.
[38] ChemAxon - software solutions and services for chemistry & Biology. https://chemaxon.com/. (Accessed 6 February 2020).
[39] F. Alix, V. Gembus, L. Coquet, M. Hubert-Roux, P. Chan, L. Truong, M. Sebban, G. Coadou, H. Oulyadi, C. Papamicaël, V. Levacher, Dihydroquinoline carbamate DQS1-02 as a prodrug of a potent acetylcholinesterase inhibitor for Alzheimer's disease therapy: multigram-scale synthesis, mechanism investigations, in vitro safety pharmacology, and preliminary in vivo toxicology profile, ACS Omega 3 (2018) 18387–18397, https://doi.org/10.1021/acsomega.8b02121.
[40] P. Bacalhau, A.A. San Juan, A. Goth, A.T. Caldeira, R. Martins, A.J. Burke, Insights into (S)-rivastigmine inhibition of butyrylcholinesterase (BuChE): molecular docking and saturation transfer difference NMR (STD-NMR), Bioorg. Chem. 67 (2016) 105–109, https://doi.org/10.1016/j.bioorg.2016.06.002.
[41] S. Deiana, C.R. Harrington, C.M. Wischik, G. Riedel, Methylthioninium chloride reverses cognitive deficits induced by scopolamine: comparison with rivastigmine, Psychopharmacology (Berl) 202 (2009) 53–65, https://doi.org/10.1007/s00213-008-1394-2.
[42] L. Robinson, A.V. Goonawardena, R. Pertwee, R.E. Hampson, B. Platt, G. Riedel, WIN55,212-2 induced deficits in spatial learning are mediated by cholinergic hypofunction, Behav. Brain Res. 208 (2010) 584–592, https://doi.org/10.1016/j.bbr.2010.01.004.
[43] G.M. Sheldrick, Phase annealing in SHELX-90: direct methods for larger structures, Acta Crystallogr. Sect. A Found. Crystallogr. 46 (1990) 467–473, https://doi.org/10.1107/S0108767390000277.
[44] G.M. Sheldrick, A short history of SHELX, Acta Crystallogr. Sect. A Found. Crystallogr. 64 (2008) 112–122, https://doi.org/10.1107/S0108767307043930.
[45] T.X. Nguyen, M. Abdelmalak, C. Marchand, K. Agama, Y. Pommier,

M. Cushman, Synthesis and biological evaluation of nitrated 7-, 8-, 9-, and 10-hydroxyindenoisoquinolines as potential dual topoisomerase I (Top 1)–Tyrosyl-DNA Phosphodiesterase I (TDP1) inhibitors, J. Med. Chem. 58 (2015) 3188–3208, https://doi.org/10.1021/acs.jmedchem.5b00136.

[46] A. Meden, D. Knez, M. Jukič, X. Brazzolotto, M. Gršič, A. Pišlar, A. Zahirović, J. Kos, F. Nachon, J. Svete, S. Gobec, U. Grošelj, Tryptophan-derived butyrylcholinesterase inhibitors as promising leads against Alzheimer's disease, Chem. Commun. 55 (2019) 3765–3768, https://doi.org/10.1039/C9CC01330J.

[47] G. Jones, P. Willett, R.C. Glen, Molecular recognition of receptor sites using a genetic algorithm with a description of desolvation, J. Mol. Biol. 245 (1995) 43–53, https://doi.org/10.1016/S0022-2836(95)80037-9.

[48] G. Jones, P. Willett, R.C. Glen, A.R. Leach, R. Taylor, Development and validation of a genetic algorithm for flexible docking, J. Mol. Biol. 267 (1997) 727–748, https://doi.org/10.1006/jmbi.1996.0897.

[49] J.C. Phillips, R. Braun, W. Wang, J. Gumbart, E. Tajkhorshid, E. Villa, C. Chipot, R.D. Skeel, L. Kalé, K. Schulten, Scalable molecular dynamics with NAMD, J. Comput. Chem. 26 (2005) 1781–1802, https://doi.org/10.1002/jcc.20289.

[50] J. Huang, A.D. MacKerell Jr., CHARMM36 all-atom additive protein force field: validation based on comparison to NMR data, J. Comput. Chem. 34 (2013) 2135–2145, https://doi.org/10.1002/jcc.23354.

[51] J. Huang, S. Rauscher, G. Nawrocki, T. Ran, M. Feig, B.L. de Groot, H. Grubmüller, A.D. MacKerell Jr., CHARMM36m: an improved force field for folded and intrinsically disordered proteins, Nat. Methods 14 (2017) 71–73, https://doi.org/10.1038/nmeth.4067.

[52] K. Vanommeslaeghe, E. Hatcher, C. Acharya, S. Kundu, S. Zhong, J. Shim, E. Darian, O. Guvench, P. Lopes, I. Vorobyov, A.D. MacKerell Jr., CHARMM general force field: a force field for drug-like molecules compatible with the CHARMM all-atom additive biological force fields, J. Comput. Chem. 31 (2010) 671–690, https://doi.org/10.1002/jcc.21367.

[53] J. Lee, X. Cheng, J.M. Swails, M.S. Yeom, P.K. Eastman, J.A. Lemkul, S. Wei, J. Buckner, J.C. Jeong, Y. Qi, S. Jo, V.S. Pande, D.A. Case, C.L. Brooks 3rd, A.D. MacKerell Jr., J.B. Klauda, W. Im, CHARMM-GUI input generator for NAMD, GROMACS, AMBER, OpenMM, and CHARMM/OpenMM simulations using the CHARMM36 additive force field, J. Chem. Theor. Comput. 12 (2016) 405–413, https://doi.org/10.1021/acs.jctc.5b00935.

[54] W.L. Jorgensen, C. Jenson, Temperature dependence of TIP3P, SPC, and TIP4P water from NPT Monte Carlo simulations: seeking temperatures of maximum density, J. Comput. Chem. 19 (1998) 1179–1186, https://doi.org/10.1002/(SICI)1096-987X(19980730)19:10<1179::AID-JCC6>3.0.CO;2-J.

[55] T. Darden, D. York, L. Pedersen, Particle mesh Ewald: an N•log(N) method for Ewald sums in large systems, J. Chem. Phys. 98 (1993) 10089–10092, https://doi.org/10.1063/1.464397.

[56] B.R. Brooks, C.L. Brooks, A.D. MacKerell, L. Nilsson, R.J. Petrella, B. Roux, Y. Won, G. Archontis, C. Bartels, S. Boresch, A. Caflisch, L. Caves, Q. Cui, A.R. Dinner, M. Feig, S. Fischer, J. Gao, M. Hodoscek, W. Im, K. Kuczera, T. Lazaridis, J. Ma, V. Ovchinnikov, E. Paci, R.W. Pastor, C.B. Post, J.Z. Pu, M. Schaefer, B. Tidor, R.M. Venable, H.L. Woodcock, X. Wu, W. Yang, D.M. York, M. Karplus, CHARMM: the biomolecular simulation program, J. Comput. Chem. 30 (2009) 1545–1614, https://doi.org/10.1002/jcc.21287.

[57] C. Lecoutey, C. Rochais, D. Genest, S. Butt-Gueulle, C. Ballandonne, S. Corvaisier, F. Dulin, A. Lepailleur, J. Sopkova-de Oliveira Santos, P. Dallemagne, J.S.O. Santos, P. Dallemagne, Synthesis of dual AChE/5-HT4 receptor multi-target directed ligands, Medchemcomm 3 (2012) 627–634, https://doi.org/10.1039/C2MD20063E.

[58] T. Freret, V. Bouet, A. Quiedeville, G. Nee, P. Dallemagne, C. Rochais, M. Boulouard, Synergistic effect of acetylcholinesterase inhibition (donepezil) and 5-HT4 receptor activation (RS67333) on object recognition in mice, Behav. Brain Res. 230 (2012) 304–308, https://doi.org/10.1016/j.bbr.2012.02.012.

[59] N. Hooper, C. Fraser, T.W. Stone, Effects of purine analogues on spontaneous alternation in mice, Psychopharmacology (Berl) 123 (1996) 250–257, https://doi.org/10.1007/BF02246579.